

New Self-Similar Solutions of Polytropic Gas Dynamics

Yu-Qing Lou^{1,2,3} * and Wei-Gang Wang¹

¹*Physics Department and Tsinghua Center for Astrophysics (THCA), Tsinghua University, Beijing, 100084, China;*

²*Department of Astronomy and Astrophysics, the University of Chicago, 5640 South Ellis Avenue, Chicago, IL 60637, USA;*

³*National Astronomical Observatories, Chinese Academy of Sciences, A20, Datun Road, Beijing 100012, China.*

Accepted 2006 ?? ?. Received 2006 ?? ??; in original form 2006 March ??

ABSTRACT

We explore semi-complete self-similar solutions for the polytropic gas dynamics involving self-gravity under spherical symmetry, examine behaviours of the sonic critical curve, and present new asymptotic collapse solutions that describe ‘quasi-static’ asymptotic behaviours at small radii and large times. These new ‘quasi-static’ solutions with divergent mass density approaching the core can have self-similar oscillations. Earlier known solutions are summarized. Various semi-complete self-similar solutions involving such novel asymptotic solutions are constructed, either with or without a shock. In contexts of stellar core collapse and supernova explosion, a hydrodynamic model of a rebound shock initiated around the stellar degenerate core of a massive progenitor star is presented. With this dynamic model framework, we attempt to relate progenitor stars and the corresponding remnant compact stars: neutron stars, black holes, and white dwarfs.

Key words: black hole physics — hydrodynamics — shock waves — stars: neutron — supernovae — white dwarfs

1 INTRODUCTION

The self-similar evolution of gas dynamics with spherical symmetry under self-gravity and thermal pressure has attracted considerable interest in contexts of various astrophysical applications [Shu (1977); Goldreich & Weber (1980); Fillmore & Goldreich (1984); Lou (2005); Hu, Shen, Lou & Zhang (2006)]. There are several reasons to pursue such model studies: numerical simulations show the tendency of self-similar behaviours in spherical flows (e.g. Bodenheimer & Sweigart 1968 and Foster & Chevalier 1993); this model framework is sufficiently simple, yet can still carry valuable information on the roles of the competing forces of gravity and thermal pressure. Larson (1969a, b) and Penston (1969a, b) were the first to analyse such similarity problems in astrophysical contexts. Since then, different asymptotic solutions and global numerical solutions have been found and developed. In the isothermal case, Shu (1977) obtained the inner free-fall asymptotic solution with divergent speed and density profiles at small x , and constructed the expansion wave collapse solution (EWCS) to suggest the inside-out collapse scenario for the formation of low-mass stars. Subsequently, Hunter (1977) discovered a sequence of discrete solutions, referred to as

the Hunter type solutions, which have finite density and speed profiles at small radii, by a matching procedure in the density-speed phase diagram. Whitworth & Summers (1985) noted the existence of asymptotic solutions of constant speed at large radii, as a generalization of the asymptotic solution at large x of Shu (1977), and constructed solutions with weak discontinuities across the sonic critical line. The properties of such weak discontinuities were further discussed by Hunter (1986). Recently, Lou & Shen (2004) constructed isothermal solutions to describe self-similar evolution of envelope expansion with core collapse (EECC) using the similar matching procedure of Hunter (1977). Bian & Lou (2005) explored various similarity isothermal shock solutions.

For a polytropic gas, Cheng (1978) introduced a generalized self-similar transformation in the sense of $\kappa \equiv p/\rho^\gamma$ being constant along each streamline but not globally, where $1 \leq \gamma \leq 5/3$ and the initial density profile may be adjusted, and mainly studied the polytropic counterparts of isothermal EWCSs. Yahil (1983) developed a model for κ being a global constant, discussed the polytropic case for $6/5 \leq \gamma \leq 4/3$, and mainly focussed on the polytropic counterparts of Hunter-type isothermal solutions. Suto & Silk (1988) used a similarity transformation similar to that of Yahil (1983), but discussed a generalization of the equation of state for $1 < \gamma < 4/3$ involving yet another parameter n , and mainly constructed the counterparts of isothermal free-

* E-mail: louyq@tsinghua.edu.cn and lou@oddjob.uchicago.edu; wwg03@mails.tsinghua.edu.cn

fall solutions both crossing and not crossing the sonic critical curve; McLaughlin & Pudritz (1997) treated the limit case of $\gamma \rightarrow 0$ using the logotropic equation of state, and considered the free-fall solutions and EWCSs as counterparts of earlier analyses. Fatuzzo, Adams & Myers (2004) explored the possibility of an initial equation of state being different from a later dynamic equation of state, and examined the dependence of the accreted mass versus the polytropic index; their self-similar solutions do not encounter the sonic critical curve. The basic polytropic model framework has also been extended in various relevant physical aspects, e.g., Terebey, Shu & Cassen (1984) for a slowly rotating gas cloud, Boily & Lynden-Bell (1995) for including various forms of radiative losses, Semelin, Sanchez & de Vega (2001) for including viscosity, Wang & Lou (2006) for modelling a random magnetic field, as well as other relevant research works involving hydrodynamic and MHD shocks (Bian & Lou 2005; Yu et al. 2006).

Among these earlier research works, Suto & Silk (1988) introduced a straightforward self-similar transformation and analyzed polytropic self-similar flows as a generalization of an isothermal gas (e.g. Shu 1977). They analyzed both cases of $\gamma > 1$, $n = 1$ and of $n = 2 - \gamma$. The $n = 1$ case is somewhat artificial because this equation of state evolves with time and does not conserve the local specific entropy. We therefore focus on the $n = 2 - \gamma$ case in this paper to explore a polytropic model for the collapse of a massive star. As shocks are ubiquitous and important in various astrophysical processes (e.g. Kennel & Coroniti 1984 for an MHD model of the Crab Nebula with shocks), and self-similar shocks have been investigated in various astrophysical contexts (e.g. Tsai & Hsu 1995; Shu et al. 2002; Shen & Lou 2004; Bian & Lou 2005; Yu, Lou, Bian & Wu 2006), we further construct self-similar shocks in a polytropic gas in this paper. We analyze the behaviour of the sonic critical curve and present new asymptotic solution referred to as the ‘quasi-static’ asymptotic solution. Semi-complete solutions containing the ‘quasi-static’ asymptotic solution as the limit are constructed, either with or without a shock. We invoke this simple theoretical framework to model the collapse of a massive progenitor star involving a rebound shock in the stellar interior, expelling stellar materials and leaving behind a remnant compact object, such as white dwarfs, neutron stars, and black holes.

This paper is arranged as follows. The general background information is provided in Section 1. Section 2 gives an account for the hydrodynamic formulation of the model problem and previously known solutions. Section 3 treats the sonic critical curve. In Section 4, we present the novel ‘quasi-static’ asymptotic solutions. We describe self-similar shocks and the relevant jump condition in Section 5. In Section 6, we show various semi-complete solutions either with or without a shock. Section 7 contains numerical examples for a rebound shock within a collapsing star. Finally in Section 8, we provide summary and conclusions.

2 FORMULATION AND KNOWN SOLUTIONS

2.1 Nonlinear Hydrodynamic Equations

The present theoretical model problem treats the self-gravitational fluid dynamics under the spherical symmetry.

Our analysis and results are applicable to the vast region sufficiently far away from the central sphere surrounding various core activities. In the spherical polar coordinates (r, θ, ϕ) , the standard nonlinear polytropic hydrodynamic equations are in the forms of

$$\frac{\partial \rho}{\partial t} + \frac{1}{r^2} \frac{\partial}{\partial r}(r^2 \rho u) = 0, \quad (1)$$

$$\frac{\partial M}{\partial t} + u \frac{\partial M}{\partial r} = 0, \quad (2)$$

$$\frac{\partial M}{\partial r} = 4\pi r^2 \rho, \quad (3)$$

$$\rho \left(\frac{\partial u}{\partial t} + u \frac{\partial u}{\partial r} \right) = -\frac{\partial p}{\partial r} - \frac{GM\rho}{r^2}, \quad (4)$$

$$p = \kappa \rho^\gamma, \quad (5)$$

where $u(r, t)$ is the radial bulk fluid velocity at radius r and time t , $\rho(r, t)$ is the gas mass density, $M(r, t)$ is the total mass enclosed within radius r at time t , $G = 6.67 \times 10^{-8} \text{ g}^{-1} \text{ cm}^{-3} \text{ s}^{-2}$ is the gravitational constant, and p is the thermal gas pressure. The Poisson equation relating the gravitational potential Φ (such that $d\Phi/dr = GM/r^2$) and ρ is consistently satisfied. In equation of state (5), the proportional coefficient κ is independent of t and is assumed to be a global constant. This κ would be the same as the notation $K(t)$ in equation (11) of Suto & Silk (1988) when the parameter n of Suto & Silk (1988) (and also in this paper to be defined presently) is equal to $2 - \gamma$. The range $1 < \gamma < 4/3$ for the polytropic index γ is adopted in our current model analysis.¹

2.2 A Self-Similar Transformation

We introduce the self-similar transformation (Suto & Silk 1988) with respect to a new dimensionless independent variable x as follows.

$$r \equiv ax, \quad u \equiv bv, \quad \rho \equiv cx, \quad p \equiv d\beta, \quad M \equiv em, \quad (6)$$

where the scaling factors $a(t)$ through $e(t)$ are defined by

$$a \equiv k^{1/2} t^n, \quad b \equiv k^{1/2} t^{n-1}, \quad c \equiv \frac{1}{4\pi G t^2},$$

$$d \equiv \frac{k t^{2n-4}}{4\pi G}, \quad e \equiv \frac{k^{3/2} t^{3n-2}}{(3n-2)G}, \quad (7)$$

with k and n being two constants. Here $v(x)$, $\alpha(x)$, $\beta(x)$ and $m(x)$ are dimensionless functions of x only. Substituting expressions (6) and (7) into the original polytropic hydrodynamic equations (1) through (5) and assuming $n = 2 - \gamma$ for a global constant $\kappa = k(4\pi G)^{\gamma-1}$, we obtain

$$m = \alpha x^2 (nx - v), \quad (8)$$

$$\alpha' = \alpha^2 \left[(n-1)v + \frac{nx-v}{3n-2} \alpha - \frac{2(x-v)(nx-v)}{x} \right] [\alpha(nx-v)^2 - \gamma\alpha^\gamma]^{-1}, \quad (9)$$

and

¹ See Appendix A for a brief discussion on cases of $\gamma \geq 4/3$.

$$v' = \left[(n-1)\alpha v(nx-v) + \frac{(nx-v)^2}{(3n-2)}\alpha^2 - 2\gamma\alpha^\gamma \frac{(x-v)}{x} \right] \left[\alpha(nx-v)^2 - \gamma\alpha^\gamma \right]^{-1}. \quad (10)$$

So far, the development is the same as that of Suto & Silk (1988) with the requirement of $n = 2 - \gamma$. From equation (8), it is clear that $nx - v > 0$ is necessary for $m > 0$ as a physical requirement for solutions.

2.3 Known Similarity Solutions

Various solutions of the two coupled nonlinear ordinary differential equations (ODEs) (9) and (10) have been known previously. These solutions with $n = 2 - \gamma$, which were first established in the isothermal case and then generalized to the polytropic case, are summarized below.

The static solution of a singular polytropic sphere (SPS) is characterized by

$$v = 0, \quad \alpha = \left[\frac{n^2}{2\gamma(3n-2)} \right]^{1/n} x^{-2/n},$$

$$m = n \left[\frac{n^2}{2\gamma(3n-2)} \right]^{1/n} x^{3-2/n}. \quad (11)$$

This is to be compared with the singular isothermal sphere (SIS; e.g., Shu 1977) and with the magnetized singular isothermal sphere (mSIS; Yu & Lou 2005).

The Larson-Penston type of solutions is generalized to

$$v = \frac{2x}{3}, \quad \alpha = \frac{2}{3}, \quad m = \frac{2(n-2/3)}{3}x^3, \quad (12)$$

which was found by Larson (1969a, b) and Penston (1969a, b) in the isothermal case with $n = 1$; this is also known as the non-relativistic Einstein de-Sitter polytropic expansion solution (see Shu et al. 2002 for the isothermal counterpart).

The asymptotic solution finite at large x is given by

$$v = \left(-\frac{nA}{3n-2} + \frac{2\gamma A^{\gamma-1}}{n} \right) x^{(n-2)/n} + Bx^{(n-1)/n},$$

$$\alpha = Ax^{-2/n}, \quad (13)$$

where A and B are two constants of integration. The isothermal counterpart solution with $B = 0$ and $n = 1$ was discussed by Shu (1977), and the more general solution containing the free parameter B was first obtained by Whitworth & Summers (1985). In this paper, asymptotic solutions with $B = 0$ and $v > 0$ as the leading term at large x is referred to as breeze solutions, asymptotic solutions with $B = 0$ and $v < 0$ as the leading term at large x is referred to as contraction solution, asymptotic solutions with $B > 0$ are referred to as outflow or wind solutions and asymptotic solutions with $B < 0$ are referred to as inflow solutions.

The leading diverging behaviour of central free-fall collapse solution in a polytropic gas at small x is characterized by

$$v = -\left[\frac{2m(0)}{(3n-2)x} \right]^{1/2},$$

$$\alpha = \left[\frac{(3n-2)m(0)}{2x^3} \right]^{1/2}, \quad (14)$$

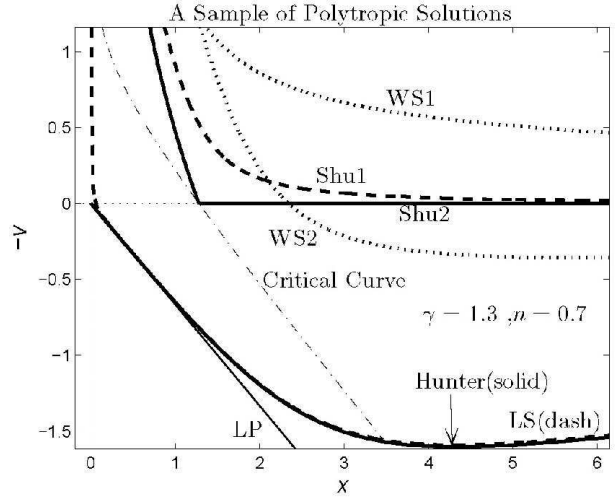


Figure 1. Polytropic hydrodynamic similarity solutions with $\gamma = 1.3$ and $n = 0.7$ as examples of illustration for the counterparts of the isothermal similarity solutions formerly constructed by various authors. The dash-dotted curve represents the sonic critical curve as defined in the text. The heavy dashed curve marked with ‘Shu1’ is a solution with a contraction at large x and a free-fall collapse at small x without crossing the sonic critical curve. The heavy solid curve marked with ‘Shu2’ is the polytropic EWCS. The two heavy dotted curves labelled by ‘WS1’ and ‘WS2’ are inflow and outflow solutions at large x with free-fall collapse at small x , respectively. The light solid solution labelled ‘LP’ represents a Larson-Penston type of polytropic solution. The heavy solid curve labelled by ‘Hunter’ is a Hunter type polytropic solution obtained by a phase matching procedure with the sonic critical point parameters $(\alpha, x, v) = (0.1641, 3.4865, 1.5711)$ and a central reduced density parameter $\alpha_* = 22.038$, and the heavy dashed curve labelled by ‘LS’ is a polytropic EECC solution first constructed by Lou & Shen (2004) for the isothermal case with two sets of relevant sonic critical point parameters $(\alpha, x, v) = (164.69, 0.002978, -2.4497)$ and $(\alpha, x, v) = (0.1639, 3.4684, 1.5586)$. The last two curves happen to be fairly close to each other when $x \gtrsim 0.1$.

with $m(x)$ approaching a finite value $m(0)$, which was first found by Shu (1977) for the isothermal case with $n = 1$.

The Hunter type of asymptotic solutions at small x are given by

$$v = \frac{2}{3}x - \frac{\alpha_*^{(1-\gamma)}}{15\gamma} \left(\alpha_* - \frac{2}{3} \right) \left(n - \frac{2}{3} \right) x^3 + \dots,$$

$$\alpha = \alpha_* - \frac{\alpha_*^{(2-\gamma)}}{6\gamma} \left(\alpha_* - \frac{2}{3} \right) x^2 + \dots, \quad (15)$$

where α^* is a constant of integration. The isothermal counterpart of this solution was first obtained by Hunter (1977) with $n = 1$ and $\gamma = 1$.

These solutions are summarized here as the polytropic counterparts of the relevant results in the isothermal case. Figure 1 is a collection of examples for previously known solutions with parameters $\gamma = 1.3$ and $n = 0.7$. The EWCS constructed here is the polytropic counterpart of the isothermal EWCS obtained by Shu (1977). Given the more general equation of state studied by Cheng (1978), the isothermal EWCS represents only a subset of all possible EWCSs (see

Table 1. Relevant parameters for the known types of global similarity polytropic solutions constructed for $n = 0.7$ and $\gamma = 1.3$ (see Figure 1) are summarized below. Parameters $m(0)$ and α_* are provided when the inner asymptotic behaviours are in the free-fall type or the Hunter type, respectively.

type	$m(0)$	A	B	α_*
Shu1	0.350	0.5	0	/
Shu2	0.273	0.5	-1	/
WS1	0.374	1	1	/
WS2	0.700	0.404413	0	/
LS	3.58×10^{-3}	2.34	3.78	/
Hunter	/	2.37	3.82	22.038

also McLaughlin & Pudritz 1997 in the logotropic approximation).

3 THE SONIC CRITICAL CURVE

The points where the denominators on the right-hand sides (RHSs) of both ODEs (9) and (10) vanish constitute the singular surface. On this surface, the travel speed of disturbances relative to the local flow speed is equal to the local sound speed. Global solutions of the two ODEs (9) and (10) cannot cross this singular surface smoothly, unless the intersection happens to (i) lie on the so-called sonic critical curve, on which both the numerators and denominators of the RHSs in the two ODEs vanish, and (ii) have the first derivatives of v and α with respect to x satisfying the critical conditions at this intersection point (see Whitworth & Summers 1985 for the isothermal case). There are possibilities to go across the sonic critical curve with weak discontinuities (e.g., Whitworth & Summers 1985) or with shocks (Tsai & Hsu 1985; Shu et al. 2002; Bian & Lou 2005; Yu, Lou, Bian & Wu 2006; Lou & Gao 2006). The sonic critical curve and the critical conditions are derived below (see also McLaughlin & Pudritz 1997).

3.1 Determination of the Sonic Critical Curve

For an isothermal gas, the sonic critical curve can be expressed in the form of v and α as functions of x (Shu 1977; Lou & Shen 2004). For a polytropic gas, the sonic critical curve can be determined numerically for x and v values from specified α values. As only two of the three vanishing equations of numerators and denominators are independent, we just need to consider the following two equations.

$$(nx - v)^2 = \gamma\alpha^{\gamma-1} \quad (16)$$

and

$$(n-1)v + \alpha \frac{(nx-v)}{(3n-2)} - \frac{2(x-v)(nx-v)}{x} = 0. \quad (17)$$

For $nx - v > 0$ and thus $m > 0$, we then obtain

$$v = nx - \sqrt{\gamma}\alpha^{(\gamma-1)/2} \quad (18)$$

and

$$\left(n-1 + \frac{\alpha}{3n-2}\right)\sqrt{\gamma}\alpha^{(\gamma-1)/2} = \frac{2\gamma}{x}\alpha^{\gamma-1} - n(n-1)x \quad (19)$$

to determine the sonic critical curve. Given a specific α value (note that $\alpha > 0$ by definition), the corresponding x values can be solved from equation (19) as

$$x = \left[n-1 + \frac{\alpha}{3n-2} \pm \sqrt{\left(n-1 + \frac{\alpha}{3n-2}\right)^2 - 8n(1-n)} \right] \times [2n(1-n)]^{-1} \sqrt{\gamma}\alpha^{(\gamma-1)/2}. \quad (20)$$

We then obtain the corresponding v from equation (18) once α and x are known.

3.2 Completeness and Asymptotic Behaviours of the Sonic Critical Curve

According to equation (19), in order to achieve a positive x value, α must be larger than a critical value α_c defined by

$$\alpha_c \equiv (3n-2)\{2[2n(1-n)]^{1/2} + 1 - n\}. \quad (21)$$

When $\alpha > \alpha_c$, equation (19) gives two different positive x roots. It is also routine to verify that when taking the ‘+’ and ‘-’ signs in equation (20), x monotonically increases and decreases with increasing α , respectively.

The asymptotic behaviours of the sonic critical curve can be inferred from equation (20). When α approaches $+\infty$ and taking the ‘+’ sign in equation (20), we have

$$x \simeq \sqrt{\gamma}\alpha^{(\gamma+1)/2} / [n(1-n)(3n-2)], \quad (22)$$

$$v \simeq nx,$$

while taking the ‘-’ sign in equation (20), we have

$$x \simeq 2\sqrt{\gamma}(3n-2)\alpha^{(\gamma-3)/2},$$

$$v \simeq -\sqrt{\gamma}\alpha^{(\gamma-1)/2} \simeq -\sqrt{\gamma} \left[\frac{x}{2\sqrt{\gamma}(3n-2)} \right]^{-(\gamma-1)/(3-\gamma)}. \quad (23)$$

Equations (22) and (23) show the asymptotic trends of v and x versus α , and is valuable in determining the entire sonic critical curve. Our analysis here is complementary to the analysis on the sonic critical points by Suto & Silk (1988).

Fig. 2 shows the sonic critical curves for different values of γ and n with $n = 2 - \gamma$. This figure shows clearly the qualitative difference in the asymptotic behaviours between the isothermal and polytropic cases.

3.3 Eigensolutions across the Sonic Critical Curve

As the sonic critical curve is a singular curve for the two nonlinear ODEs (9) and (10), it is essential to determine the solution behaviours in the vicinity of this curve. Suto & Silk (1988) analyzed the solution behaviours in the vicinity of the sonic critical curve and obtain

$$(1+\gamma)v'^2 + \left[n+1-4\gamma+4(\gamma-1)\frac{v}{x} \right] v' + 2(2\gamma-1)\frac{v^2}{x^2} + 2\left[\frac{\alpha}{(3n-2)} - 2n-4\gamma+4 \right] \frac{v}{x} + \frac{(n-2)}{(3n-2)}\alpha + 2(n+2\gamma-2) = 0 \quad (24)$$

and

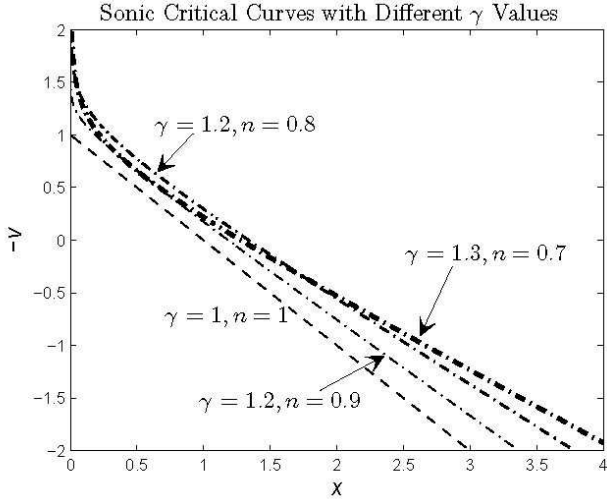


Figure 2. The sonic critical curves for different pairs of γ and n values. Here, $n = 2 - \gamma$ is adopted for a conventional polytropic gas. The $\gamma = n = 1$ line (the dashed line) is a straight line $v = x - 1$ for the isothermal case (Shu 1977; Lou & Shen 2004). The major differences between isothermal and polytropic asymptotic behaviours are the divergent behaviour at small x and the different slope of $-v$ versus x at large x of the polytropic cases.

$$\alpha' = \frac{\alpha v' - 2\alpha(x-v)/x}{(nx-v)}, \quad (25)$$

where the data set of (x, v, α) is along the sonic critical curve and v' and α' are the first-order derivatives of v and α with respect to x across the sonic critical curve. In general, there exist two eigensolutions, each corresponding to a pair of first-order derivatives v' and α' , that can cross the sonic critical curve. Whitworth & Summers (1985) constructed solutions crossing the critical curve with first-order derivatives satisfying equations (24) and (25) for the isothermal case, but with discontinuities in higher order derivatives. Hunter (1986) promptly pointed out that such solutions involve weak discontinuities and may not be physically valid. In terms of global solutions, we shall mainly consider analytically smooth solutions that cross the sonic critical curve.

4 NEW ‘QUASI-STATIC’ ASYMPTOTIC SOLUTIONS

We now describe the new ‘quasi-static’ asymptotic solutions in the present model framework.

4.1 Singular Polytropic Sphere (SPS) and Quasi-Static Asymptotic Solutions

The static solution of a singular polytropic sphere (SPS) is well known and is given by

$$v = 0, \quad \alpha = \left[\frac{n^2}{2\gamma(3n-2)} \right]^{-1/n} x^{-2/n}, \quad (26)$$

as a thermal-gravitational equilibrium (Suto & Silk 1988; note that $n = 2 - \gamma$ here). Shu (1977) used this solution to construct the so-called expansion wave collapse solution (EWCS) for the isothermal case with $n = 1$. We realize

that this solution can in fact serve as an asymptotic ‘quasi-static’ solution when x becomes sufficiently small. In other words, the leading terms of $v(x)$ and $\alpha(x)$ are described by equation (26), yet there may exist higher order terms to form an asymptotic series solution.

To be consistent, we assume up to the second orders

$$v = Lx^K = o(x) + \dots, \quad (27)$$

$$\alpha = \left[\frac{n^2}{2\gamma(3n-2)} \right]^{-1/n} x^{-2/n} + \Delta\alpha + \dots,$$

where L and K above, and N below are three constants,

$$\Delta\alpha \equiv Nx^{K-1-2/n} = o(\alpha), \quad (28)$$

with the notation $o(\alpha)$ indicating $\Delta\alpha/\alpha \rightarrow 0$ as $x \rightarrow 0^+$. Here, K may be complex in general (see the analysis below) and $Re(K) > 1$ is required such that the additional terms in equations (27) and (28) are indeed higher order terms² as compared to solution (26).

Substituting these expressions into equations (9) and (10) for small x , we obtain respectively

$$\frac{n^2(K+1)N}{2} = \left[\frac{n^2}{2\gamma(3n-2)} \right]^{-1/n} L,$$

$$n(K-1)N = \left(K + 2 - \frac{2}{n} \right) \left[\frac{n^2}{2\gamma(3n-2)} \right]^{-1/n} L, \quad (29)$$

leading to

$$K^2 - (4/n - 3)K + 2 = 0 \quad (30)$$

and

$$N = \frac{2}{n^2(1+K)} \left[\frac{n^2}{2\gamma(3n-2)} \right]^{-1/n} L. \quad (31)$$

Equation (31) shows that once a K root is determined, the ratio N/L is then obtained. Of course, L and N can also be both zero, corresponding to the static SPS solution (26).

The two K roots of quadratic equation (30) are

$$K = \frac{2}{n} - \frac{3}{2} \pm \frac{1}{2} \left(1 - \frac{24}{n} + \frac{16}{n^2} \right)^{1/2}. \quad (32)$$

For $Re(K) > 1$, $n < 0.8$ is required. When $n \leq 12 - 8\sqrt{2}$, K is a real number, while for $12 - 8\sqrt{2} < n < 0.8$, K becomes a complex number.

4.2 Quasi-Static Solutions of the First Kind with a Real K

The ‘quasi-static’ solution with a real K is apparent and is confined to a narrow range of n values, i.e., $n \leq 12 - 8\sqrt{2}$. There exist two sets of such solutions corresponding to the two K roots of equation (32) being both larger than 1. In such cases, the two asymptotic solution are of the form

$$v = Lx^K,$$

$$\alpha = \left[\frac{n^2}{2\gamma(3n-2)} \right]^{-1/n} x^{-2/n}$$

² Note that in solution (26), the first-order term of v is viewed to be $0x$ as a linear function of x .

$$+ \frac{2L}{n^2(1+K)} \left[\frac{n^2}{2\gamma(3n-2)} \right]^{-1/n} x^{K-1-2/n}, \quad (33)$$

where the two K roots are given by expression (32) and L is an arbitrary parameter.

4.3 Quasi-Static Solutions of the Second Kind with a Complex K

The ‘quasi-static’ solution with a complex K (i.e., when $12 - 8\sqrt{2} < n < 0.8$) appears special. For a complex $K = K_1 + iK_2$ with K_1 and K_2 both being real, we should take the real parts of both sides of equations (27) and (28) for real $v(x)$ and $\alpha(x)$. Then the $v(x)$ solution appears as

$$v = \text{Re}(Lx^K) = \text{Re}[Lx^{K_1} \exp(iK_2 \ln x)] \\ = x^{K_1} [L_1 \cos(K_2 \ln x) - L_2 \sin(K_2 \ln x)], \quad (34)$$

where L_1 and L_2 are real and imaginary parts of parameter L , respectively. By equation (32), we have $K_1 = 2/n - 3/2$ and $K_2 = (-1/4 + 6/n - 4/n^2)^{1/2}$ respectively. The corresponding second-order term $\Delta\alpha$ is

$$\Delta\alpha = \frac{2}{n^2} \left[\frac{n^2}{2\gamma(3n-2)} \right]^{-1/n} [(1+K_1)^2 + K_2^2]^{-1} x^{-5/2} \\ \times \left\{ [L_1(1+K_1) + L_2K_2] \cos(K_2 \ln x) \right. \\ \left. - [L_2(1+K_1) - L_1K_2] \sin(K_2 \ln x) \right\}. \quad (35)$$

Since the relative phase factor in both expressions (34) and (35) can be adjusted by choosing the two free parameters L_1 and L_2 , there is no loss of generality to adopt a positive value of K_2 .

5 SELF-SIMILAR SHOCKS AND POLYTROPIC JUMP CONDITIONS

Shocks form when faster flows catch up slower flows. In our model, it is of considerable interest to discuss self-similar shocks with the shock front ‘fixed’ in the self-similar profile. Across such a shock front, the upstream and downstream regions experience a change in the specific entropy leading to a change in k parameter in similarity transformation (6) and (7).

5.1 Jump Conditions for Polytrropic Shocks

We denote the upstream (i.e., a fluid flows from this side into a shock front) physical variables with subscript 1, and the downstream (i.e., a fluid flows on this side away from a shock front) physical variables with subscript 2. The location of a shock front is denoted with a subscript s

$$r_s = k^{1/2} t^n x_s, \quad (36)$$

where k is for the upstream region, i.e. $k_1 = k$ or $\kappa_1 = \kappa$. For $\kappa_2 = \kappa\lambda^2$ or $k_2 = k\lambda^2$ with λ^2 being a scaling parameter, the similarity transformation in the downstream side is then

$$r_2 \equiv a_2 x_2, \quad u_2 \equiv b_2 v_2, \quad \rho_2 \equiv c_2 \alpha_2,$$

$$p_2 \equiv d_2 \beta_2, \quad M_2 \equiv e_2 m_2, \quad (37)$$

where the five time-dependent scaling functions a_2 to e_2 are defined explicitly by

$$a_2 \equiv \lambda k^{1/2} t^n, \quad b_2 \equiv \lambda k^{1/2} t^{n-1}, \quad c_2 \equiv \frac{1}{4\pi G t^2}, \\ d_2 \equiv \lambda^2 \frac{k t^{2n-4}}{4\pi G}, \quad e_2 \equiv \lambda^3 \frac{k^{3/2} t^{3n-2}}{(3n-2)G}. \quad (38)$$

At the shock front, we should have $r_1 = r_2 = r_s$ and thus

$$x_1 = x_s = \lambda x_2. \quad (39)$$

Given x_1 , v_1 and α_1 , we need only to calculate the corresponding x_2 , v_2 and α_2 across a shock, and the parameter λ is automatically determined by equation (39) and hence the downstream transformation (37) and (38) is known.

We now describe the jump conditions for shocks in a polytropic gas. Using the standard procedure, we choose the framework of reference in which the shock front is instantly at rest. The jump conditions in this shock framework of reference are then given below. The mass conservation is

$$[\rho(u_s - u)]_1^2 = 0, \quad (40)$$

where $u_s \equiv dr_s/dt$ is the radially outward travel speed of the shock front and, following the notational convention, we denote the difference of the corresponding physical variables between the upstream and downstream sides by enclosing them within a pair of square brackets with a superscript 2 and a subscript 1. The momentum conservation is

$$[\kappa\rho^\gamma + \rho(u_s - u)^2]_1^2 = 0. \quad (41)$$

The energy conservation becomes

$$\left[\frac{\rho(u_s - u)^3}{2} + \frac{\gamma\kappa(u_s - u)}{(\gamma - 1)} \rho^\gamma \right]_1^2 = 0. \quad (42)$$

Combining equations (40), (41) and (42) together with the self-similar transformation, we derive three shock conditions in terms of the self-similar variables

$$\alpha_1(n x_1 - v_1) = \lambda \alpha_2(n x_2 - v_2), \quad (43)$$

$$\alpha_1^\gamma + \alpha_1(n x_1 - v_1)^2 = \lambda^2 [\alpha_2^\gamma + \alpha_2(n x_2 - v_2)^2], \quad (44)$$

$$(n x_1 - v_1)^2 + \frac{2\gamma}{(\gamma - 1)} \alpha_1^{\gamma-1} \\ = \lambda^2 \left[(n x_2 - v_2)^2 + \frac{2\gamma}{(\gamma - 1)} \alpha_2^{\gamma-1} \right]. \quad (45)$$

5.2 Shock Solutions by the Jump Conditions

By introducing new variables $\Gamma_i \equiv n - x_i/v_i$ with $i = 1, 2$, we reduce equations (43) through (45) to

$$\alpha_1 \Gamma_1 = \alpha_2 \Gamma_2, \quad (46)$$

$$\frac{\alpha_1^\gamma}{x_1^2} + \alpha_1 \Gamma_1^2 = \frac{\alpha_2^\gamma}{x_2^2} + \alpha_2 \Gamma_2^2, \quad (47)$$

$$\Gamma_1^2 + \frac{2\gamma}{(\gamma - 1)} \frac{\alpha_1^{\gamma-1}}{x_1^2} = \Gamma_2^2 + \frac{2\gamma}{(\gamma - 1)} \frac{\alpha_2^{\gamma-1}}{x_2^2}. \quad (48)$$

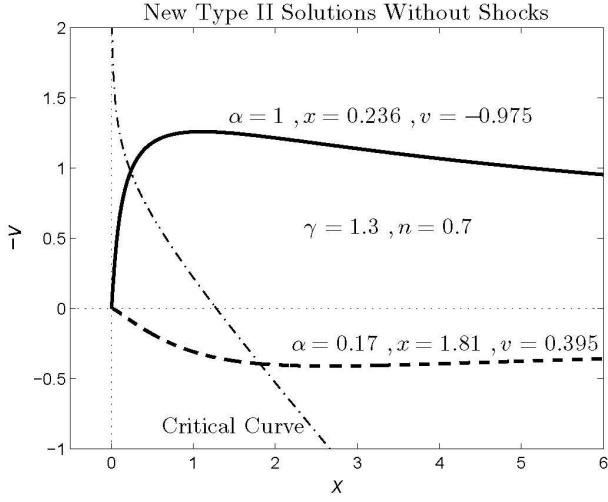


Figure 3. Semi-complete similarity solutions approaching type II ‘quasi-static’ asymptotic solutions at small x without shocks for $\gamma = 1.3$ and $n = 0.7$. Here, $-v$ versus x is shown. The dash-dotted line is the sonic critical curve. The solid solution is an inflow solution which is obtained by integrating from $(x, v, \alpha) = (0.236, -0.975, 1)$ on the critical curve inward; and the dashed curve is an outflow solution which is obtained by integrating from $(x, v, \alpha) = (1.81, 0.395, 0.17)$ on the critical curve inward. The two dotted straight lines are the abscissa and ordinate axes, respectively. For a sufficiently small x , both solutions approach the Type II ‘quasi-static’ asymptotic solution.

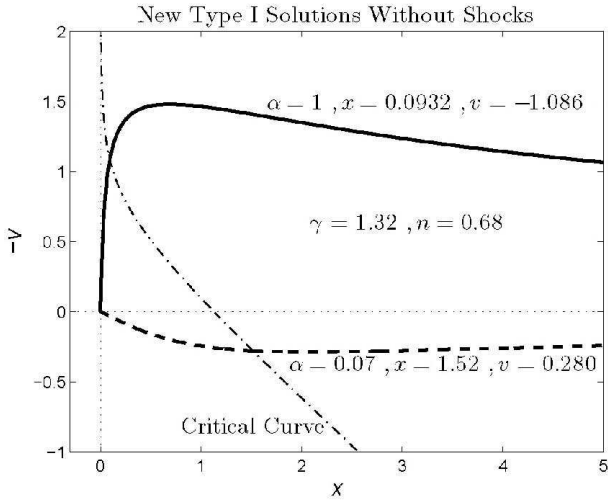


Figure 4. Semi-complete similarity solutions approaching type I ‘quasi-static’ asymptotic solutions at small x without shocks for $\gamma = 1.32$ and $n = 0.68$. Here, $-v$ versus x is shown. The dash-dotted line is the sonic critical curve. The solid curve is an inflow solution which is obtained by integrating from $(x, v, \alpha) = (0.0932, -1.086, 1)$ on the sonic critical curve inward; and the dashed curve is an outflow solution obtained by integrating from $(x, v, \alpha) = (1.52, 0.280, 0.07)$ on the sonic critical curve inward. The two dotted straight lines are the abscissa and ordinate axes, respectively. For a sufficiently small x , both solutions approach the Type I ‘quasi-static’ asymptotic solution.

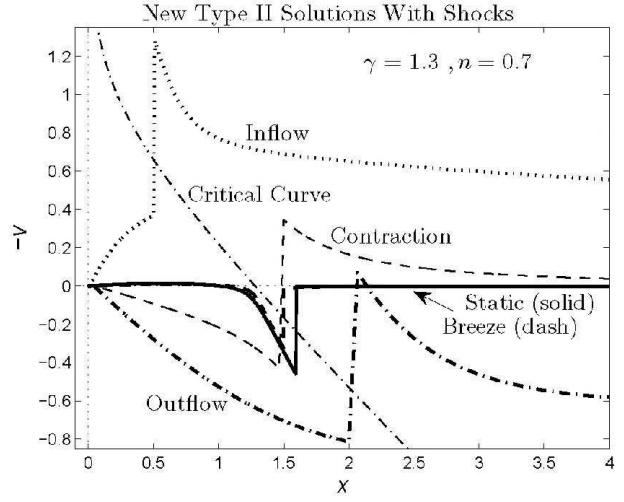


Figure 5. Semi-complete similarity shock solutions containing Type II ‘quasi-static’ asymptotic solutions for $\gamma = 1.3$ and $n = 0.7$ are shown here in terms of $-v$ versus x . The heavy dotted curve is a shock solution with an inflow in the outer portion, constructed by integrating from $(x, v, \alpha) = (0.751, -0.426, 0.3)$ on the sonic critical curve with $x_{s_2} = 0.5$; the heavy dash-dotted line is a solution with an outflow in the outer portion, constructed by integrating from $(x, v, \alpha) = (2.47, 0.866, 0.16)$ on the sonic critical curve with $x_{s_2} = 2$; the light dashed curve is a solution with a contracting outer portion, constructed with parameters $A = 0.5$, $B = 0$ and a chosen $x_{s_1} = 1.5$; the heavy solid curve is a solution with a static outer portion (i.e., part of a SPS), constructed with parameters $A = 0.404$, $B = 0$ and a chosen $x_{s_1} = 1.6$; the heavy dashed curve is a shock solution with a breeze in the outer portion, constructed with parameters $A = 0.402$ and $B = 0$ and choosing $x_{s_1} = 1.5$. The two light dotted straight lines are the abscissa and ordinate axes, respectively. For small x , all solutions approach the Type II ‘quasi-static’ asymptotic solution.

We intend to solve for Γ_2 , α_2 and x_2 with known values of Γ_1 , α_1 and x_1 . By substituting $\alpha_2 = \alpha_1 \Gamma_1 / \Gamma_2$ of equation (46), solving for x_2^2 from equations (47) and (48) respectively, and eliminating x_2^2 accordingly, we arrive at the following quadratic equation in terms of Γ_2

$$\frac{(\gamma + 1)}{2\gamma} \Gamma_2^2 - \frac{(\alpha_1^\gamma / x_1^2 + \alpha_1 \Gamma_1^2)}{\alpha_1 \Gamma_1} \Gamma_2 + \frac{(\gamma - 1)}{2\gamma} \left(\Gamma_1^2 + \frac{2\gamma}{\gamma - 1} \frac{\alpha_1^{\gamma-1}}{x_1^2} \right) = 0. \quad (49)$$

Excluding the trivial solution $\Gamma_2 = \Gamma_1$, we obtain one root of equation (49) in the form of

$$\Gamma_2 = \frac{2\gamma \alpha_1^{\gamma-1}}{(\gamma + 1) x_1^2 \Gamma_1} + \frac{(\gamma - 1)}{(\gamma + 1)} \Gamma_1. \quad (50)$$

In terms of the upstream Mach number \mathcal{M}_1 defined by

$$\mathcal{M}_1^2 \equiv \frac{(u_s - u_1)^2}{s_1^2} = \frac{\rho_1 (u_s - u_1)^2}{\gamma p_1} = \frac{x_1^2 \Gamma_1^2}{\gamma \alpha_1^{\gamma-1}}, \quad (51)$$

expression (50) reads

$$\frac{u_s - u_2}{u_s - u_1} = \frac{\Gamma_2}{\Gamma_1} = \frac{2}{(\gamma + 1) \mathcal{M}_1^2} + \frac{(\gamma - 1)}{(\gamma + 1)}; \quad (52)$$

this is precisely equation (89.6) of Landau & Lifshitz (1959).

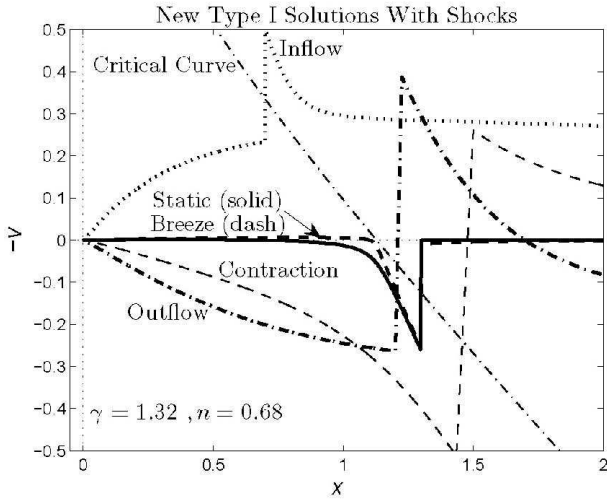


Figure 6. Semi-complete similarity shock solutions containing Type I ‘quasi-static’ asymptotic solutions for $\gamma = 1.32$ and $n = 0.68$ are shown in terms of $-v$ versus x . The heavy dotted line is a solution with an inflow in the outer portion, constructed by integrating from $(x, v, \alpha) = (0.812, -0.243, 0.1)$ on the sonic critical curve with a chosen $x_{s_2} = 0.7$; the heavy dash-dotted line is a solution with an outflow in the outer portion and constructed by integrating from $(x, v, \alpha) = (1.52, 0.280, 0.07)$ on the sonic critical curve with a chosen $x_{s_2} = 1.2$; the light dashed curve is a solution with a contracting envelope, constructed with parameters $A = 0.15$ and $B = 0$ and a chosen $x_{s_1} = 1.5$; the heavy solid curve is a solution with a static outer portion of SPS, constructed with parameters $A = 0.114$ and $B = 0$ and a chosen $x_{s_1} = 1.3$; the heavy dashed curve is a solution with a breeze in the outer portion, constructed with parameters $A = 0.1135$ and $B = 0$ and a chosen $x_{s_1} = 1.3$. The two dotted straight lines are the abscissa and ordinate axes, respectively. All solutions approach the Type I ‘quasi-static’ asymptotic solution at small x .

It is straightforward to prove that the following set of inequalities are compatible with each other (\mathcal{M}_2 is the downstream Mach number)

$$\begin{aligned} \frac{\Gamma_2}{\Gamma_1} < 1, \quad \frac{u_s - u_2}{u_s - u_1} < 1, \quad \mathcal{M}_1^2 > 1, \quad \mathcal{M}_2^2 < 1, \\ \lambda > 1, \quad k_2 > k_1, \quad \kappa_2 > \kappa_1. \end{aligned} \quad (53)$$

We only give a proof for the compatibility between $\lambda > 1$ and $\mathcal{M}_1^2 > 1$ below as an example of illustration. First note that when $\mathcal{M}_1^2 > 1$, we have $z \equiv \Gamma_2/\Gamma_1 < 1$. From equation (47), we then solve for $\lambda^2 = x_1^2/x_2^2$ as

$$\lambda^2 = z^\gamma [\gamma \mathcal{M}_1^2 (1 - z) + 1] = \frac{2\gamma(1 - z)z^\gamma}{(\gamma + 1)z - (\gamma - 1)} + z^\gamma. \quad (54)$$

The first derivative of λ^2 with respect to z gives

$$\frac{d\lambda^2}{dz} = -\frac{\gamma(\gamma^2 - 1)(z - 1)^2 z^{\gamma-1}}{[(\gamma + 1)z - (\gamma - 1)]^2} < 0 \quad (55)$$

for $\gamma > 1$. Since $\lambda^2 \rightarrow 1$ as $z \rightarrow 1$, it follows that when $z < 1$ (i.e., $\mathcal{M}_1^2 > 1$), $\lambda > 1$ holds and vice versa. According to the Zemplén theorem [see, e.g., Landau & Lifshitz (1959)], for entropy to increase across a shock going from the upstream to downstream side, we have physical shock solutions with $u_s - u_2 < u_s - u_1$. While this general conclusion only holds

for weak shocks, it is true in our case from equivalent inequalities (53). That is, the upstream and downstream regions should be supersonic and subsonic, respectively.

5.3 Solutions and Physical Interpretation

For the convenience of analysis and comprehension, we adopt the solution procedure and presentation in the following manner. We do not distinguish between x_1 and x_2 in the unshocked regions, even though the self-similar transformations are different for the upstream and downstream sides, respectively. We use x_{s_1} and x_{s_2} for the shock location under the similarity transformations of the upstream and downstream sides, respectively. The ratio $\lambda = x_{s_1}/x_{s_2}$ is then fixed by shock jump conditions. In figure illustrations of shock solutions, we juxtapose curves for $-v_1$ versus x_1 and for $-v_2$ versus x_2 in the same figure, with the implied differences in downstream and upstream transformations, and link the two shock points $(-v_{s_1}, x_{s_1})$ and $(-v_{s_2}, x_{s_2})$ by a straight line, indicating that these two points represent the demarcation of upstream and downstream quantities on the two sides of the shock front, respectively. A reader of these figures may interpret the curves to the left of this straight line ($x < x_{s_2}$) as inner downstream solutions, and the curves to the right of this straight line ($x > x_{s_1}$) as the corresponding outer upstream solutions. As several shock solutions are pact together within one figure, one should also note that for different shock solutions, this demarcation is also different because x_s values are different. The advantage of such presentations is that the critical curve of both regions coincide in the figure, i.e., the curve provided in these figures serves as the critical curve in both regions. Furthermore, one can obtain the x_{s_1} and x_{s_2} values directly from the figure to compute λ values accordingly. In our figures, the scalings of physical quantities are different in the presentation for upstream and downstream regions, and the scalings are only for the reduced quantities. For example, one unit in the two regions of the figure represents the same difference of x values, but not the same difference of r values; the situation is similar in terms of the correspondence between v and u values.

Once we obtain a shock solution as described above, the procedure of obtaining a physical solution of our hydrodynamic model is to assign a k value of either region, i.e., k_1 or k_2 , and obtain the k value for the other region by the simple relation $k_2 = k_1 \lambda^2$. With the separate self-similar transformations in the upstream and downstream regions, we readily compute the corresponding physical quantities of the solution. In the dimensional form, the difference in the scaling of physical quantities due to the similarity transformations disappears. For example, $r_{s_1} = r_{s_2}$ now, and a unit in the two regions in the figures represents the same difference of r values.

6 SEMI-COMPLETE SOLUTIONS WITH THE ‘QUASI-STATIC’ ASYMPTOTIC BEHAVIOURS

Semi-complete similarity solutions include those that do not intersect with the singular surface, that go across the sonic point analytically, and that cross the sonic critical curve

Table 2. Parameters A , B and L of asymptotic behaviours for solutions without shocks presented in Figures 3 and 4.

n	type	A	B	L
0.7	outflow	0.673	0.852	$1.11 + 0.735i$
0.7	inflow	0.0840	-2.27	$-11.4 + 19.7i$
0.68	outflow	0.176	0.573	0.452
0.68	inflow	0.0142	-2.55	-301

Table 3. Parameters A , B and L of asymptotic behaviours and shock parameters x_{s_1} , x_{s_2} and λ for global similarity shock solutions approaching type II ‘quasi-static’ asymptotic behaviours at small x as shown in Figure 5.

type	A	B	L	x_{s_2}	x_{s_1}	λ
inflow	0.227	-1.15	$2.09 - 0.841i$	0.5	0.511	1.022
outflow	1.19	1.56	$3.57 + 1.87i$	2	2.07	1.034
contraction	0.5	0	$0.289 + 0.188i$	1.46	1.5	1.024
SPS	0.404	0	$0.00233 - 0.0973i$	1.59	1.6	1.0058
breeze	0.402	0	$-0.00207 - 0.0562i$	1.497	1.5	1.0018

with shocks in the region $0 < x < +\infty$ (see Lou & Shen 2004; Bian & Lou 2005; Yu et al. 2006). Either with or without shocks, semi-complete solutions approaching the ‘quasi-static’ asymptotic behaviours at small x are constructed in the present model. Specifically, we are able to construct self-similar shock solutions approaching the ‘quasi-static’ asymptotic behaviours at small x yet with inflow, outflow, SPS, breeze or contraction in the outer envelope. In this section, we choose $n = 0.7$ and $n = 0.68$ for type II and type I ‘quasi-static’ asymptotic behaviours at small x , respectively.

6.1 Smooth Similarity Solutions without Shocks

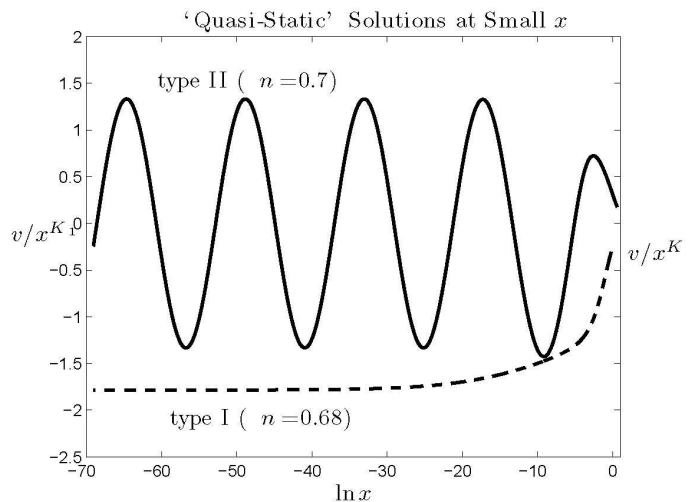
We are able to construct semi-complete similarity solutions without shocks simply by integrating inward from a certain point on the sonic critical curve, using the analytical eigensolution with a smaller v' in the close vicinity of this chosen point [equations (24) and (25) determine the eigensolution]. Figures 3 and 4 are examples of illustration for semi-complete similarity solutions without shocks, approaching type II and type I ‘quasi-static’ solutions at small x , respectively. In Figure 4, only similarity solutions with smaller K values in equation (32) are constructed by integrating from the sonic critical curve using one of the eigensolutions.

6.2 Similarity Solutions with Shocks

Based on the jump conditions, we are able to construct similarity shock solutions with inflow, outflow, breeze, SPS or contraction in the outer portion, connected to either type II or type I ‘quasi-static’ asymptotic solutions at small x . In constructing semi-complete shock solutions with inflow or outflow for the outer asymptotic behaviours, we use an inner solution that can cross the sonic critical curve smoothly by integrating inward from the sonic critical curve using an eigensolution, choose an x_{s_2} value in the downstream region along this inner solution, determine the upstream quantities by the shock jump conditions, and integrate outward

Table 4. Parameters A , B and L for asymptotic behaviours and shock parameters x_{s_1} , x_{s_2} and λ for similarity shock solutions with type I ‘quasi-static’ asymptotic behaviours shown in Fig. 6.

type	A	B	L	x_{s_2}	x_{s_1}	λ
inflow	0.0765	-0.498	-1.78	0.7	0.7009	1.0013
outflow	0.184	0.412	0.452	1.2	1.225	1.021
contract	0.15	0	-0.203	1.43	1.5	1.046
static	0.114	0	-0.0196	1.298	1.3	1.0018
breeze	0.1135	0	-0.0248	1.298	1.3	1.0015


Figure 7. ‘Quasi-static’ asymptotic solutions for small x values. The presentation is in the v/x^K versus $\ln x$ form for type I ‘quasi-static’ asymptotic solution, and in the v/x^{K_1} versus $\ln x$ form for type II ‘quasi-static’ asymptotic solution. The type I solution is obtained by integrating inward from $(x, v, \alpha) = (0.812, -0.243, 0.1)$ on the sonic critical curve, and the type II solution is obtained by integrating inward from $(x, v, \alpha) = (1.81, 0.395, 0.17)$ on the sonic critical curve.

from x_{s_1} for the outer part of the solution. On the other hand, in order to construct similarity solutions with breeze, SPS or contraction in the outer portions, we integrate inward from a large x value (say 10^5) to reach a certain value x_{s_1} , determine the downstream quantities and integrate further inward to small x values. Only when the inner solutions approach the ‘quasi-static’ asymptotic solution do we succeed in constructing such global shock solutions. Figures 5 and 6 are examples of illustration for self-similar shock solutions approaching type II and type I ‘quasi-static’ asymptotic behaviours at small x , respectively. In both Figs. 5 and 6, examples of inflow, outflow, contraction, breeze and SPS for outer portions are illustrated. For type I ‘quasi-static’ asymptotic solutions, we again obtain solutions only with smaller K values in equation (32).

6.3 Asymptotic Behaviours of Sample Solutions

All solutions presented in this section approach the ‘quasi-static’ (either type I or type II) asymptotic behaviours at small x values. Figure 7 displays two examples illustrating such asymptotic behaviours in terms of v/x^K versus $\ln x$ for

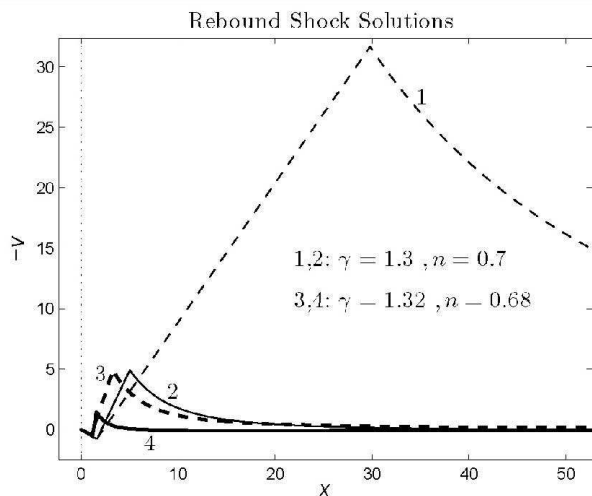


Figure 8. Sample shock solutions for polytropic gas dynamics. Solutions 1 and 2 are obtained by integrating inward from $(x, v, \alpha) = (2.533, 0.9074, 0.1598)$ on the sonic critical curve and choosing $x_{s_2} = 1.6198$ and $x_{s_2} = 1.64$, respectively. Solutions 3 and 4 are obtained by integrating inward from $(x, v, \alpha) = (1.793, 0.4374, 0.067)$ on the sonic critical curve and choosing $x_{s_2} = 1.1$ and $x_{s_2} = 1.2$, respectively. The relevant parameters for asymptotic behaviours and for shock conditions are summarized in Table 5. The two dotted straight lines are abscissa and ordinate axes, respectively. The straight lines in the middle represent shocks, and the two x_s values correspond to the same r_s .

Table 5. Parameters for asymptotic solutions and shocks in the polytropic shock solutions displayed in Figure 8.

No.	1	2	3	4
γ	1.3	1.3	1.32	1.32
A	3920	23.5	5.40	0.493
B	-0.00442	0.562	-0.792	0.371
L	$3.83 + 2.27i$	$3.84 + 2.28i$	0.441	0.441
x_{s_1}	29.79	5.013	3.288	1.578
x_{s_2}	1.6198	1.64	1.1	1.2
λ	18.39	3.056	2.989	1.315

type I solution and v/x^{K_1} versus $\ln x$ for type II solution. For the type II 'quasi-static' solution, the sine (cosine) pattern is apparent, while for the type I 'quasi-static' solution, the tendency to a constant value is also fairly clear. For the convenience of comparison and reference, we also list all the relevant parameters x_{s_1} , x_{s_2} and λ for shocks and A , B and L for asymptotic behaviours in Tables 2, 3 and 4.

7 SELF-SIMILAR REBOUND SHOCKS IN CORE COLLAPSING STARS

7.1 Physical Scenario

The core collapse of a massive star involves a multitude of physical processes of nuclear burning, radiation pressure, degenerate materials, electrons, and neutrinos (Hirata et al. 1987; Bionta et al. 1987; Bethe 1993). Here, we only consider several gross aspects from the point of view of fluid dynamics involving self-gravity and try to outline a free-fall

core collapse and a rebound shock scenario for a supernova explosion.

At the onset of gravitational core collapse inside a massive star, the central region suddenly loses pressure and a nearly free infall towards the center ensues; meanwhile, the information of core collapse travels outward through the stellar interior to reach the envelope and a self-similar collapse phase grossly characterized by asymptotic free-fall solution (14) at small $x \propto r/t^n$ may gradually emerge. By physical estimates, this happens on a timescale of a few seconds. For small x , we obtain³ the radial flow speed $u \propto -t^{(3n/2)-1}r^{-1/2}$, the mass density $\rho \propto t^{(3n/2)-2}r^{-3/2}$, the enclosed mass $M \rightarrow k^{3/2}m(0)t^{3n-2}/[(3n-2)G]$, and the core mass accretion rate $\dot{M} \rightarrow k^{3/2}m(0)t^{3(n-1)}/G$ with $n > 2/3$. It should be noted that before the onset of core collapse, the progenitor star is expected to have a wind in general and the star itself can engage in global oscillations, be they acoustic p -modes or internal gravity g -modes. For example, for purely radial stellar acoustic oscillations, the stellar envelope and interior can move radially either outward or inward depending on the phase of oscillation during the rapid core collapse. These plausible physical conditions may lead to different self-similar evolution behaviours during a free-fall core collapse. Also, the material degeneracy can already set in the core well before the onset of gravitational core collapse. Moreover, the mass density divergence associated with the free-fall collapse solution (14) can rapidly trigger core degeneracy. In reality, no infinity should arise.

As mass accumulates towards the center, singularity arises mathematically and similarity disappears. As the degenerate core pressure rapidly builds up to resist the material infall, a powerful rebound shock emerges around the core and drives out most gas materials as it ploughs through the infalling stellar envelope, leaving behind a remnant compact object (such as a neutron star or a black hole⁴) with high mass density in the degenerate core. For instance, for the formation of a neutron star, the breakout of such a rebound shock through the stellar photosphere is crucial to initiate a supernova explosion observed at terrestrial observatories (e.g., Bethe 1995; Burrows 2000 and Lattimer & Prakash 2004 for reviews of supernova and neutron star physics and extensive references therein). Again, we propose that after the emergence of a rebound shock around the collapsing core, a self-similar evolution grossly characterized by either 'quasi-static' asymptotic solution (33) or quasi-static' asymptotic solution (34) and (35) may gradually appear and persist as the rebound shock travel outward against infalling materials. The self-similar evolution phase of a rebound shock may last on timescales in the range of $\sim 10^4 - 10^5$ s or longer.

³ Bethe (1993) indicated $u \propto r^{-1/2}$ and $\rho \propto t^{-1}r^{-3/2}$ outside the (rebound) shock and after the start of (core) collapse. This would correspond to an index $n = 2/3$; for a conventional polytropic gas with $n = 2 - \gamma$, this would in turn imply $\gamma = 4/3$ for an extremely relativistically hot gas (e.g., Goldreich & Weber 1980). We take $n > 2/3$ in our model framework to make the enclosed mass M physically meaningful in self-similar transformation (7).

⁴ We will also discuss the possibility of producing or exposing a white dwarf in a similar process separately. For a low-mass progenitor star, the formation of a proto-white dwarf in the core may or may not involve a violent rebound shock explosion.

For ‘quasi-static’ asymptotic solution (33) of the first type at small x , we have $u = Lk^{(1-K)/2}t^{-n(K-1)-1}r^K$, $\rho \propto r^{-2/n} + \epsilon t^{-n(K-1)}r^{K-2/n}$, $M \propto r^{3-2/n}$, and $\dot{M} \propto Lt^{-n(K-1)-1}r^{K+2-2/n}$, where $L < 0$ for an inflow, $K > 1$, and ϵ is a sufficiently small parameter. In other words, the radial flow speed u decreases with time and approaches zero as $r \rightarrow 0$; the mass density ρ diverges as $r \rightarrow 0$ to induce material degeneracy; being independent of time t , the enclosed mass M vanishes as $r \rightarrow 0$; and the core mass accretion rate \dot{M} decreases with time and approaches zero as $r \rightarrow 0$ by quadratic equation (32). A very important and testable prediction of this first type of self-similar rebound shock explosions is that the mass density ρ for stellar materials scales as $r^{-2/n}$ with $2/n < 3$ behind the rebound shock after a sufficiently long lapse of time; for a conventional polytropic gas with $n = 2 - \gamma$ and $\gamma \geq 1$, we would also have $2 < 2/n$. Ideally, this mass density profile can be better preserved with a more or less quiet central nonrotating neutron star or Schwarzschild black hole, otherwise central activities or winds inevitably destroy central part of the density profile. An immediate example comes to mind is the Cassiopeia A supernova remnant which appears more or less spherical with a nonrotating X-ray bright neutron star left behind (i.e., no X-ray pulsations are detectable so far by *Chandra* satellite observations).

For ‘quasi-static’ asymptotic solution (34) and (35) of the second type (with logarithmic oscillations) at small $x \equiv r/(k^{1/2}t^n)$, we then have the radial flow speed $u = k^{(1-K_1)/2}t^{-n(K_1-1)-1}r^{K_1}[L_1 \cos(K_2 \ln x) - L_2 \sin(K_2 \ln x)]$, the mass density $\rho \propto r^{-2/n} + \eta t^{(5n-4)/2}r^{-5/2}\{[L_1(1 + K_1) + L_2K_2] \cos(K_2 \ln x) - [L_2(1 + K_1) - L_1K_2] \sin(K_2 \ln x)\}$, the enclosed mass $M \propto r^{3-2/n}$, the core mass accretion rate $\dot{M} \propto k^{(1-K_1)/2}t^{-n(K_1-1)-1}r^{1/2}[L_1 \cos(K_2 \ln x) - L_2 \sin(K_2 \ln x)]$, where η is a readily identifiable coefficient, L_1 and L_2 are two small parameters, $K_1 = 2/n - 3/2$, $K_2 = (-1/4 + 6/n - 4/n^2)^{1/2}$ and $n > 2/3$. In reference to the first type of self-similar ‘quasi-static’ asymptotic solutions (33), the qualitative distinction of this second type of self-similar ‘quasi-static’ asymptotic solutions (34) and (35) is of course the oscillatory feature. The overall strength of this oscillatory feature tends to die out with increasing time t . Nevertheless, at a given time t , the mass density profile of ρ may still retain a considerable oscillatory feature especially for small r or small x . Again, we propose to use the data of the Cassiopeia A supernova remnant or other suitable supernova remnants to identify or search for such oscillatory features. A series of our self-similar shock solutions with ‘quasi-static’ asymptotic solutions of first and second types are consistent, at least qualitatively, to the major features of such a plausible rebound shock scenario for supernova explosions.

To be more specific and tangible, we present a series of self-similar rebound shock solutions approaching central ‘quasi-static’ asymptotic solutions in Figure 8. They serve as examples of illustration for a possible hydrodynamic similarity model of a rebound shock in a core collapsing progenitor star. Among various physical possibilities, these rebound shocks are constructed as such, because we would like to demonstrate similarity shock solutions with (i) an inflow right on the upstream side of the shock, which accounts for the creation of a rebound shock propagating outward through a collapsing envelope; (ii) a self-similar shock,

modelling a rebound shock after encountering a highly compressed over-dense core in a gravitational collapse; (iii) a massive outward expansion behind (downstream of) the rebound shock, such that gas materials of the massive progenitor star are driven out by such a powerful bouncing; and (iv) a ‘quasi-static’ asymptotic behaviour at small x , so that eventually the dense inner core comes to a near equilibrium as time goes on. These four features are qualitatively consistent with the rebound shock scenario of a perceived supernova explosion, leaving a compact object behind. We show shock solutions with both type I (solutions 3 and 4) and type II (solutions 1 and 2) ‘quasi-static’ asymptotic solutions at small x , because both satisfy the above intuitive physical requirements qualitatively. Solutions 1 and 3 have inflowing outer portions, while solutions 2 and 4 have outflowing outer portions⁵ to encompass various conceivable situations. In principle, there may also exist contracting and breezing outer portions with other features much alike the core collapse situations just described above.

7.2 Spatial and Temporal Cutoffs

For a massive progenitor star, the self-similar evolution of a core collapsing process with a rebound shock cannot persist all the time and thus a temporal or spatial cutoff needs to be specified. However, the similarity model is characterized by a continuous mass density profile with no natural cutoffs present in solutions themselves. We thus refer to astronomical data to estimate a sensible boundary for our model application. In this model, we set a radius r_i (for instance, $r_i = 10^6$ cm if the compact object is a neutron star or black hole, and $r_i = 10^8$ cm if it is a white dwarf) for our sample solutions; and we choose a radius r_o (for example, $r_o \equiv 10^{12}$ cm) as the outer boundary for application of our sample solutions. A typical massive star has a radius of the order of $\simeq 10^{12}$ cm (see Herrero et al. 1992 and Schönberner & Harmanec 1995 for observational data on masses and radii of main-sequence O and B stars). In principle, we could invoke even larger stellar radii for even more massive stars.

For these spatial cutoffs, the cutoff time is introduced below accordingly. A rebound shock emerges roughly around the core of a massive star when the collapse produces an over-dense degenerate core. It travels outward and evolves into a self-similar phase. We take the time when the shock crosses the inner radius (say, $\sim 10^6$ cm for a neutron star radius) as the initial time to apply our shock solution. This time would then correspond to

$$t_1 = \left(\frac{r_i}{k_1^{1/2} x_{s1}} \right)^{1/n}. \quad (56)$$

Here, t_1 is obtained assuming our model to be valid from the beginning at $t = 0$. This estimate also roughly represents the time needed for the shock to evolve from the center to the inner reference radius r_i . Specific estimates of t_1 are summarized in Table 7 with adopted parameters indicated. Since our ‘quasi-static’ asymptotic solution approaches a static state as $t \rightarrow +\infty$, we do not set an upper bound in time for our rebound shock model.

⁵ The progenitor star may oscillate radially prior to and during the onset of a gravitational core collapse as already noted earlier.

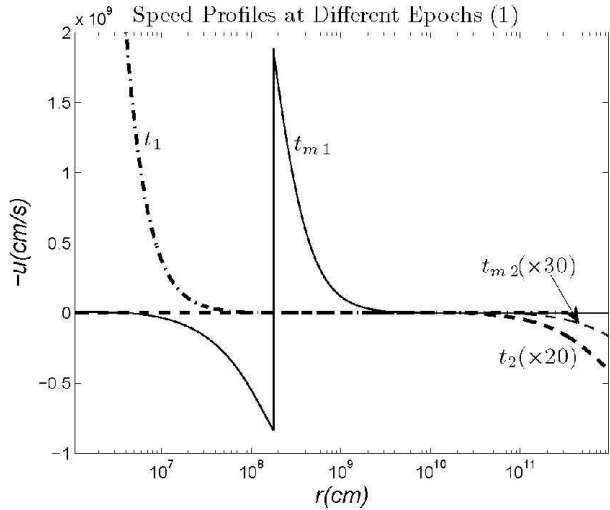


Figure 9. The negative radial flow speed profile $-u$ at different time t values of the numerical example, with r in the logarithmic scale, for the model 1 in Figure 8. Here, $t_1 = 6.15 \times 10^{-5}$ s is the time when the shock crosses the inner radius r_i , $t_2 = 2.29 \times 10^4$ s is the time when the shock crosses the outer boundary r_o ; $t_{m1} = 0.1$ s and $t_{m2} = 10^5$ s are intermediate times between t_1 and t_2 , and between t_2 and $t = \infty$, respectively. Negative radial speed profiles have been multiplied by various numerical factors shown in the figure for the compactness and clarity of presentation.

7.3 Properties of Rebound Shock Solutions

We note a common property of self-similar rebound shock solutions shown in Figure 8. As $x \rightarrow +\infty$ and as $x \rightarrow 0^+$, the profiles of radial flow speed u and mass density ρ both become independent of time t . For a specified radial range of r within a star, the stellar configurations are either static or stationary both at the beginning ($t \rightarrow 0^+$) and at the end ($t \rightarrow +\infty$). In particular, the enclosed mass is given by

$$M = \frac{nk^{1/n}A}{(3n-2)G} r^{3-2/n} \quad (57)$$

for asymptotic solutions at large x , whereas

$$M = \frac{n}{(3n-2)G} \left[\frac{k2\gamma(3n-2)}{n^2} \right]^{1/n} r^{3-2/n} \quad (58)$$

for the ‘quasi-static’ asymptotic solutions of both types at small x .

These analytical results may be utilized to grossly estimate mass variations of a star during the core collapse and supernova explosion processes. As t approaches 0^+ , if one takes our model to be valid from the beginning, then the enclosed stellar mass M is known once a progenitor stellar radius r_o is specified. Likewise, if one takes our model to be valid after a sufficiently long time (i.e., $t \rightarrow +\infty$), a quasi-static core equilibrium is ultimately achieved and the enclosed mass M is known for a specified core radius r_i .

A summary of the estimated enclosed mass values for both the outer stellar radius r_o and the inner reference radius r_i for solutions presented above are given in Table 6 for the four rebound shock solutions in Fig. 8. We refer to the enclosed mass at $t \rightarrow 0^+$ as the initial mass (hence the subscript ini), and the enclosed mass at $t \rightarrow +\infty$ as the ultimate mass (hence the subscript ult), respectively. The initial

Table 6. The adopted k values and the initial and ultimate enclosed mass values for the four models shown in Figure 8. The subscript o denotes the outer enclosed mass, and subscript i denotes the inner enclosed mass; while subscript ini represents the initial mass, and ult represents the ultimate mass.

No.	1	2	3	4
k_1 (cgs units)	8.87×10^{14}	3.21×10^{16}	3.36×10^{16}	1.735×10^{17}
k_2 (cgs units)	3×10^{17}	3×10^{17}	3×10^{17}	3×10^{17}
$M_{i,ini}(M_\odot)$	3.35	3.38	3.11	3.18
$M_{i,ult}(M_\odot)$	1.42	1.42	1.65	1.65
$M_{o,ini}(M_\odot)$	24.1	24.3	7.02	7.17
$M_{o,ult}(M_\odot)$	10.2	10.2	3.71	3.71

mass may roughly represent the mass of a progenitor star just evolved into a self-similar phase after the initiation of a core collapse, and the ultimate mass may roughly correspond to the mass of the remnant compact object as a long time has elapsed. The determination of the k values in both the upstream (subscript 1) and downstream (subscript 2) regions are described in the next subsection; while the inner and outer radii are set to be $r_i = 10^6$ cm and $r_o = 10^{12}$ cm here for considering remnant neutron stars or black holes.

7.4 Estimates for values of k Parameter

Clearly, once the numerical value of the k parameter in similarity transformation (6) and (7) is determined for a star, the shock model is then specified. Since

$$k = \frac{p}{\rho^\gamma (4\pi G)^{\gamma-1}} = \frac{Nk_B T}{\bar{m}\rho^{\gamma-1} (4\pi G)^{\gamma-1}}, \quad (59)$$

where N is the particle number density, \bar{m} is the mean molecular (atomic) mass of the gas particle, and the second equality holds only for an ideal gas, we may in principle determine k parameter using the physical quantities in equation (59). Nevertheless, even for long-studied main-sequence stars, the determination of physical parameters in the stellar interior has been challenging, not to mention the relevant parameters for massive collapsing stars, which involve various rapid physical processes and are extremely rare to be caught in action. Currently, some theoretical estimates of such parameters are available, although most of these parameters are estimated for static configurations, e.g., main-sequence stars or neutron stars. These two stellar configurations as part of our model considerations, are the progenitor star and the remnant compact object left behind a rebound shock, respectively. While the value of k parameter is by no means constant during complicated processes before and after the similarity evolution involving a constant k , we would presume for simplicity that the k value does not change significantly during the dynamical evolution.

Appenzeller & Tscharnuter (1974), Bond, Arnett & Carr (1984), Nadyozhin & Razinkova (2005) and Schaller et al. (1992) gave theoretical estimates for the hydrogen-burning phase of massive stars with $\rho_c \sim 1$ g/cm³ and $T_c \sim 10^7$ – 10^8 K. Using $\bar{m} = 0.5m_p$ with m_p being the proton mass, we obtain approximately $k \sim 10^{17}$ cgs units. Arnett (1977), Bond et al. (1984),

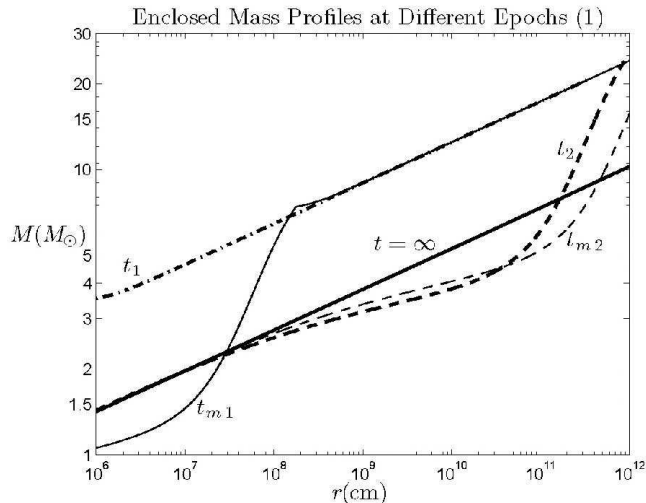


Figure 10. The total enclosed mass at different time t values of the numerical example in logarithmic scales, for the first model in Figure 8. Here, $t_1 = 6.15 \times 10^{-5}$ s is the time when the shock crosses the inner radius r_i , $t_2 = 2.29 \times 10^4$ s is the time as the shock crosses the outer boundary r_o ; $t_{m1} = 0.1$ s and $t_{m2} = 10^5$ s are intermediate time values between t_1 and t_2 , and between t_2 and $t = \infty$, respectively.

and Schaller et al. (1992) provided theoretical predictions for the late evolution phase of massive stars after the hydrogen-burning phase, and the results are $\rho_c \sim 10^8$ g/cm³ and $T_c \sim 10^9$ K. Using these late-phase parameters and $\bar{m} = 4m_p/3$ for helium atoms, we derive $k \sim 10^{16}$ cgs units. Also from the equation of state for degenerate neutrons, the corresponding $p_c \sim 10^{35}$ dynes/cm² and $\rho_c \sim 10^{15}$ g/cm³ may be appropriate for neutron stars (e.g., Shapiro & Teukolsky 1983), and the estimated k value is accordingly $\sim 10^{17}$ cgs units.

In the rebound shock model construction as we intend to discuss applications to SNe and the formation of remnant neutron stars, we may first assign k_2 values for a reasonable enclosed mass range around $\sim 1M_\odot$. To be consistent with estimates for typical neutron stars, the k_2 value is estimated to be $\sim 3 \times 10^{17}$ cgs units for both type I and type II ‘quasi-static’ asymptotic solutions at small x . The value of k_1 is derived accordingly for each shock model, using the λ parameter from the shock jump conditions. The k values thus determined in our shock models are summarized in Table 6. We see that all the k_1 values are of the orders of $\sim 10^{15\sim 17}$ cgs units, fairly close to the estimates for massive progenitor stars.

7.5 Shock Model Presentation

Figs. 9 and 10, as well as Figs. 11 and 12 present the profiles of the negative radial flow speed $-u$ and the enclosed mass M at different temporal epochs, respectively.

Besides the timescale t_1 as the initial time of our model, we introduce another typical timescale t_2 which is the time when the shock reaches the outer radius r_o , namely

$$t_2 = \left(\frac{r_o}{k_1^{1/2} x_{s1}} \right)^{1/n}. \quad (60)$$

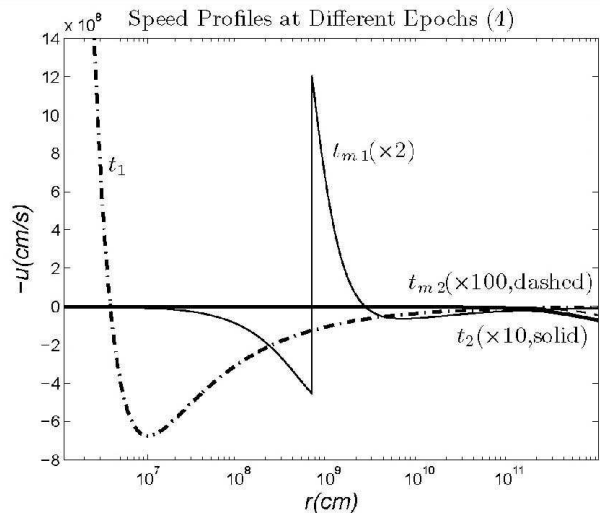


Figure 11. The radial speed profile at different time t values of the numerical example in logarithmic scales for the fourth model in Figure 8. Here, $t_1 = 7.18 \times 10^{-5}$ s is the time as the shock crosses the inner radius r_i , $t_2 = 4.78 \times 10^4$ s is the time as the shock crosses the outer boundary r_o ; $t_{m1} = 1$ s and $t_{m2} = 10^6$ s are intermediate times between t_1 and t_2 , and between t_2 and $t = \infty$, respectively. The speed profiles have been multiplied by various factors as shown for the compactness and clarity of the presentation,

Table 7. Below all time t in seconds and all enclosed mass in unit of the solar mass M_\odot . Here, t_1 for the time as the shock reaches the inner boundary and t_2 for the time as the shock reaches the outer boundary and the corresponding M_i and M_o for the four models in Figure 8. Enclosed masses for t_{m1} and t_{m2} as indicated in relevant figures are also included. The k parameters are according to Table 6.

No.	1	2	3	4
t_1	6.15×10^{-5}	6.04×10^{-5}	8.16×10^{-5}	7.18×10^{-5}
t_2	2.29×10^4	2.25×10^4	5.44×10^4	4.78×10^4
M_{i1}	3.53	3.54	3.22	3.23
M_{i2}	1.43	1.43	1.69	1.69
M_{o1}	24.1	24.3	7.03	7.17
M_{o2}	25.4	25.4	7.24	7.28
M_{im1}	1.06	1.06	1.85	1.85
M_{im2}	1.43	1.43	1.68	1.68
M_{om1}	24.1	24.3	7.03	7.17
M_{om2}	15.6	15.6	5.78	5.78

We presume our model to be valid since $t \rightarrow 0^+$. The specific t_2 values relevant to various shock models are also contained in Table 7 with adopted parameters clearly indicated. As a rebound shock cannot be seen from the Earth until the shock reaches the stellar photosphere and our outer boundary is set for the radius of a massive star, this time value roughly corresponds to the time for a rebound shock to travel out and be seen.

Quantities at five different epochs: t_1 , t_2 , $t = \infty$ and two intermediate times t_{m1} and t_{m2} are shown in the radial range $r_i = 10^6$ cm $< r < r_o = 10^{12}$ cm in Figs. 9, 10, 11 and 12. The corresponding radial flow speeds of model 2 are like those of model 4, and the corresponding radial flow

speeds of model 3 are like those of model 1. Meanwhile, the corresponding enclosed mass distributions of model 2 are like those of model 1, and the corresponding enclosed mass distributions of model 3 are like those of model 4.

7.6 Analysis of the Rebound Shock Model

We now describe model 1 results as an example of illustration. Relevant data of this model as well as other models are summarized in Tables 6 and 7. Initially, the stellar interior is in a core collapse (inflow) stage, which is triggered by the exhaustion of the central nuclear fuel. The initial profile is also significantly over-dense as compared to the eventual quasi-static configuration after a long lapse in time. The outer envelope remains collapsing as the rebound shock emerges around the central degenerate core and travels outward. The shock travels faster than the sound speed and the perturbation information cannot reach the outer region until the shock reaches there. At time t_1 , the enclosed mass within r_o is $24.1M_\odot$ and within r_i , it is $3.53M_\odot$.

The rebound shock then breaks out from the stellar interior, travelling at a fantastic speed (mostly in the range of $10^7 \sim 10^9$ cm/s). During the first few seconds, the core mass decreases rapidly. At time $t_{m1} = 0.1$ s, the enclosed mass within r_i has reduced to $1.06M_\odot$, while within r_o the enclosed mass is still $24.1M_\odot$ because the time difference is small and the mass accretion is not significant. When the shock reaches the outer boundary, a slight accretion has changed the total enclosed mass within r_o to $25.4M_\odot$, yet the inner core has already experienced a minor accretion due to radial speed oscillation of our type II ‘quasi-static’ asymptotic solution, and the enclosed mass within the inner radius r_i has now increased to $1.43M_\odot$.

After the rebound shock passes over the outer reference radius r_o , it is now the time for the massive star to drive out a significant amount of mass. As the drive gradually weakens, the total enclosed mass within r_o at time $t_{m2} = 10^5$ s falls to $15.6M_\odot$, while within r_i the total enclosed mass remains $1.43M_\odot$ as before. Eventually the enclosed mass within r_o becomes $10.2M_\odot$, and within r_i , it becomes $1.42M_\odot$. From the core mass variation and the remaining core mass within the inner reference radius r_i in the end, we reasonably conjecture that the remnant core may become a proto-neutron star. The rebound shock velocity also conforms with usual estimates.

7.7 Mass Ratio Evolution

One interesting aspect of our rebound shock model is the ratio of the initial outer mass $M_{o,ini}$, roughly corresponding to the initial mass of a prescribed progenitor star, and the ultimate inner mass $M_{i,ult}$, roughly corresponding to the mass of a remnant compact object in the core. By equations (57) and (58), this mass ratio is simply

$$\frac{M_{o,ini}}{M_{i,ult}} = \frac{A}{\lambda^{2/n}} \left[\frac{n^2}{2\gamma(3n-2)} \right]^{1/n} \left(\frac{r_o}{r_i} \right)^{(3-2/n)}. \quad (61)$$

In expression (61), the last factor involving the ratio r_o/r_i which is somewhat arbitrary, although we can estimate proper radii for different progenitor stars and ultimate compact core objects in a sensible range. The ratio of the two

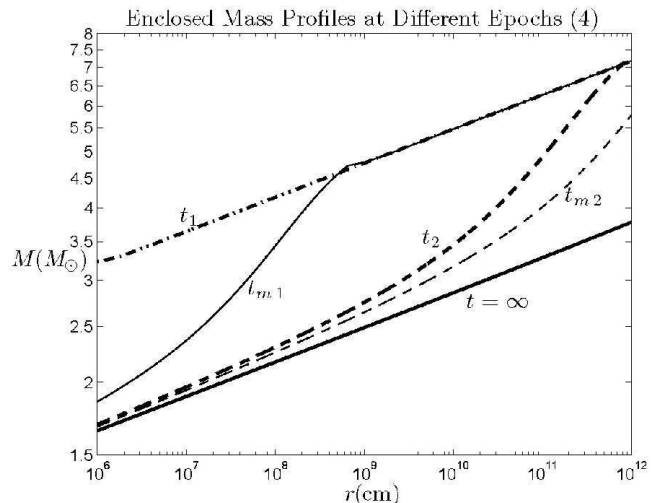


Figure 12. The total enclosed mass at different time t values of the numerical example, in logarithmic scales for the first model in Figure 8. Here, $t_1 = 7.18 \times 10^{-5}$ s is the time when the shock crosses the inner reference radius r_i , $t_2 = 4.78 \times 10^4$ s is the time as the shock crosses the outer boundary r_o ; $t_{m1} = 11$ s and $t_{m2} = 10^6$ s are intermediate time values between t_1 and t_2 , and between t_2 and $t = \infty$, respectively.

radii naturally affects the mass ratio, but as n approaches $2/3$, or equivalently γ approaches $4/3$, this last factor would approach unity. The two factors together in front of this somewhat arbitrary last factor in expression (61) is the ratio of the initial mass and the final mass within the same radius (i.e., the last factor is 1 in this case). This can vary when γ or equivalently n varies, but it also depends on x_{s2} or (x_0, v_0, α_0) , which is the point on the sonic critical curve from which we construct the ‘quasi-static’ portion of our rebound shock solutions (see subsection 6.2). Since the relation of λ and A is explored numerically, we here only provide the corresponding results for several cases with $n = 0.68$ (see Table 8), and the cases with other n or γ values are fairly similar.

According to numerical results of Table 8, mass ratio (61) increases for smaller α_0 or for larger x_{s2} . This is conceivable, in the sense that as α_0 becomes smaller, the ‘quasi-static’ portion of the rebound shock solution has a higher v for more mass being driven out; and when x_{s2} becomes smaller, the outer portion has a higher v for more mass being driven out. Referring to Table 8 and the relevant definitions therein, we also infer empirically that ratio 1 may approach 1, but whether this ratio 1 can be arbitrarily large is unclear. It appears that the choice of self-similar rebound shock solutions affects the mass ratio in a significant manner. We infer from this feature that in reality the mass ratio may also vary, and thus a compact object with a definite mass may possibly come from progenitor stars with different initial masses.

8 REMNANT PROTO-WHITE DWARFS

Conventionally, one does not invoke a rebound shock explosion to expose the degenerate core, a proto-white dwarf, of a progenitor star. It is a general belief that various mass loss

Table 8. Evolution of mass ratio $M_{o,ini}/M_{i,ult}$ for various parameters when $\gamma = 1.32$ and $n = 0.68$ are specified. For each value of α_0 , the point from which we construct our rebound shocks, we explore two cases, namely, rebound shock solutions with contracting and expanding envelopes: in the neighbouring two sets with the same α_0 values, the one with smaller x_{s_2} gives an expanding envelope, and the one with smaller x_{s_2} gives a contracting envelope. In this Table, ratio 1 is the first two factors together in expression (61), namely, $A\{n^2/[\lambda^2 2\gamma(3n-2)]\}^{1/n}$, and ratio 2 is the last factor in expression (61), namely, $(r_o/r_i)^{(3-2/n)}$.

α_0	x_{s_2}	λ	A	ratio 1	ratio 2
0.067	1.2	1.315	0.493	1.933	4.357
0.067	1.1	2.989	5.401	1.893	4.266
0.070	1.1	1.064	0.2048	1.497	3.373
0.070	0.9	1.737	0.8338	1.442	3.250
0.072	1	1.0628	0.1808	1.326	2.989
0.072	0.8	1.843	0.879	1.277	2.878
0.074	1	1.0248	0.149	1.216	2.742
0.074	0.8	1.262	0.2662	1.178	2.655
0.076	1	1.0100	0.1326	1.130	2.546
0.076	0.8	1.1238	0.1766	1.099	2.478
0.078	1	1.00383	0.1219	1.0575	2.384
0.078	0.8	1.0663	0.1422	1.0329	2.328
0.079	1	1.0000235	0.1175	1.0308	2.323
0.079	0.8	1.0496	0.1320	1.00440	2.264

mechanisms through winds are responsible for eventually producing or exposing proto-white dwarfs. However, given our theoretical framework outline in this paper, it is not obvious why a rebound shock cannot occur to blow away stellar envelope and produce a proto-white dwarf. After all, a progenitor star of mass $\sim 6 - 8M_\odot$ has to throw away a mass amount of $\sim 4.6 - 6.6M_\odot$ in order to expose a proto-white dwarf in the core.

To consider the formation of a proto-white dwarf in the degenerate core of a progenitor star in the high-mass end (say, $\sim 6 - 8M_\odot$), we would set r_i to be a typical radius of several thousand kilometers (say, $\sim 3 \times 10^8$ cm) for a white dwarf and $r_o \sim 10^{13}$ cm to be the stellar radius to enclose a mass in the range of $\sim 6 - 8M_\odot$ for the corresponding progenitor star. After the initiation of core collapse and as a powerful self-similar rebound shock travels outward, the masses enclosed within r_i and r_o decrease, sometimes oscillate, and eventually approach finite values with the increase of time t . If the final mass $M_{i,ult}$ within r_i is less than the Chandrasekhar mass limit of $1.4M_\odot$, we would say that a proto-white dwarf is produced in the remnant core. Otherwise if the final mass $M_{i,ult}$ within r_i is greater than $1.4M_\odot$, say $\sim 2 - 3M_\odot$, we would then hypothesize that dynamical instabilities associated with a proto-white dwarf exceeding the Chandrasekhar mass should have already happened before reaching the final model state of $t \rightarrow +\infty$ or $x \rightarrow 0^+$; for this to occur, the timescales of such dynamical instabilities should be shorter than the timescale of self-similar evolution around r_i . Such dynamical instabilities can give rise to a neutron star. This might then be viewed as a two-stage process to produce a neutron star with a progenitor mass roughly in the range of $\sim 6 - 8M_\odot$ or higher.

For progenitor stars with masses less than $\sim 6 - 8M_\odot$, similar rebound shocks may occur but with weaker

strengths. Such rebound shocks could fail to do the driving completely as a result of various energy losses, yet their presence and signatures may be detectable.

We now explore a few more examples for producing proto-white dwarfs or proto-neutron stars in core collapse and rebound shock processes. For all these cases below, we now take $r_i = 3 \times 10^8$ cm and $r_o = 10^{13}$ cm.

The relevant parameters for the first rebound shock model are: $n = 0.7$ (or equivalently $\gamma = 1.3$), $\alpha_0 = 0.175$, $x_0 = 1.672$, $v_0 = 0.293$, $x_{s_2} = 1.1$, $\lambda = 1.133$, $A = 0.752$, $B = -0.222$, $k_2 = 1.65 \times 10^{17}$ cgs unit, $k_1 = 1.29 \times 10^{17}$ cgs unit, $M_{o,ini} = 7.85M_\odot$, $M_{i,ult} = 1.36M_\odot$. This is a case of producing a remnant proto-white dwarf near the Chandrasekhar mass limit of $M_{i,ult} = 1.36M_\odot$ from a progenitor star of mass $M_{o,ini} = 7.85M_\odot$. We feel that with more physical input and requirements, our model can provide sensible dynamic constraints on the initial and final masses of progenitor and of remnant proto-white dwarf.

The relevant parameters for the second rebound shock model are: $k_2 = 2.2 \times 10^{17}$ cgs unit, $k_1 = 1.71 \times 10^{17}$ cgs unit, $M_{o,ini} = 11.8M_\odot$, $M_{i,ult} = 2.05M_\odot$; other parameters are the same as the first model parameters above. As already noted earlier, this proto-white dwarf may be subject to dynamical instabilities and could lead to the formation of a proto-neutron star in the end.

The relevant parameters for the third model are: $n = 0.7$ (or equivalently $\gamma = 1.3$), $\alpha_0 = 0.196$, $x_0 = 1.324$, $v_0 = 0.0341$, $x_{s_2} = 0.8$, $\lambda = 1.146$, $A = 0.5585$, $B = -0.864$, $k_2 = 2.1 \times 10^{17}$ cgs unit, $k_1 = 1.60 \times 10^{17}$ cgs unit, $M_{o,ini} = 7.96M_\odot$, $M_{i,ult} = 1.92M_\odot$. Again, this proto-white dwarf may be subject to dynamical instabilities and could lead to the formation of a proto-neutron star eventually.

9 DISCUSSION AND SPECULATIONS

We are able to construct various semi-complete self-similar solutions either with or without a rebound shock; these solutions may be adaptive to various astrophysical settings. Our numerical examples may be interpreted as an approximate model of a rebound shock initiated during the gravitational core collapse in a massive star, which drive materials out to eventually form possible quasi-static configurations.

For the convenience and clarity of discussion, we mainly focus on rebound shocks for supernovae and remnant neutron stars in the preceding sections. In fact, we may well choose a larger value of k_2 for shock models 3 and 4 in Figure 8, say, 5 times larger, it follows that all the masses and radial flow speeds should be multiplied by the same factor of 5. Then the initial progenitor mass for these two shock models would be around $35M_\odot$ and the final mass enclosed within r_i would be $8.25M_\odot$. This then implies a black hole left behind as the remnant compact object during the core collapse and rebound shock processes⁶. In addition, we can also choose relevant parameters to model the formation of white dwarfs, for instance, taking $r_i = 3 \times 10^8$ cm and $r_o = 10^{13}$ cm, we can construct an example for $M_{o,ini} = 6.3M_\odot$ and $M_{i,ult} = 1.1M_\odot$. Although we provide quantitative examples using our rebound shock model framework, our main

⁶ Brown & Bethe 1994 suggested supernova produced low-mass black holes with masses only slightly above $1.5M_\odot$.

motivation is to point out various conceptual possibilities seemingly physically plausible. After all, our current hydrodynamic model is very limited in many ways.

While we cannot draw sure conclusions on the fate of progenitor stars, we may outline a scheme for possible remnant compact objects left behind based on the current theoretical knowledge. Within the inner reference radius $r_i \sim 10^6$ cm, the final static configuration is assumed to be a proto-neutron star if the enclosed mass is in the range of $\lesssim 3 - 4M_\odot$ or a black hole if the enclosed mass is higher than $\sim 4M_\odot$; by the same token, within the inner reference radius $r_i \sim 3 - 4 \times 10^8$ cm, the final static configuration is assumed to be a proto-white dwarf if the enclosed mass is in the range of $\lesssim 1.4M_\odot$ or a proto-neutron star if the enclosed mass is higher $\sim 1.4M_\odot$.

Our analysis on the sonic critical curve shows that the critical curve has qualitative differences as compared to that of the isothermal case (e.g., Shen & Lou 2004), i.e., at small x values the sonic critical curve diverges here, and there exists a lower limit of the reduced density α on the sonic critical curve. Such analysis is technically useful in determining the sonic critical curve, and is also adaptive in determining the asymptotic behaviours of other complicated functions.

The ‘quasi-static’ asymptotic solution is so named after the first-order of this solution (viz., the semi-complete global SPS solution 11 or 26). This new asymptotic solution at small x is a characteristic of polytropic flows only. For the first type of this ‘quasi-static’ asymptotic solution with a real $K > 1$, since L can be either positive or negative, the perturbation on the SPS can be either outflow or inflow and influences the density profile correspondingly (density perturbation is positive for an outflow and negative for an inflow). The second type of this ‘quasi-static’ asymptotic solution with complex K represents a wave-like perturbation imposed on a SPS. Both the radial flow speed and density profiles have an oscillatory feature, and according to equations (34) and (35), the oscillatory terms have a phase difference not larger than $\pi/4$ between density and velocity profiles. The $x^{K_1} \exp(iK_2 \ln x)$ term in radial flow speed profile has an interesting property that the vibration decreases when x gets smaller.

In the context of supernova explosions, we propose to search for characteristic signatures in density profiles of both types of such ‘quasi-static’ asymptotic solutions in the Casiopeia A supernova remnant as well as other suitable supernova remnants. While unconventional, we suspect that some proto-white dwarfs are also formed involving rebound shocks and explosions.

Since various other physical conditions, such as the neutrino opacity, radiation pressure, general relativistic effects, magnetic field, and rotational effects are generally involved in such core collapsing phase of stellar evolution, we hope that this scenario and interpretation, while limited by a highly idealized model framework, catch some essential features of supernova explosion. This scenario should be tested by observations and numerical simulations. We plan to incorporate a random magnetic field into this model framework. Thus a parallel analysis of a magnetohydrodynamic model similar to Yu & Lou (2005) and Yu et al. (2006) is anticipated.

ACKNOWLEDGMENTS

This research has been supported in part by the ASCI Center for Astrophysical Thermonuclear Flashes at the University of Chicago, by the Special Funds for Major State Basic Science Research Projects of China, by the Tsinghua Center for Astrophysics, by the Collaborative Research Fund from the National Science Foundation of China (NSFC) for Young Outstanding Overseas Chinese Scholars (NSFC 10028306) at the National Astronomical Observatories, Chinese Academy of Sciences, by the NSFC grants 10373009 and 10533020 at the Tsinghua University, and by the SRFDP 20050003088 and the Yangtze Endowment from the Ministry of Education at the Tsinghua University. Affiliated institutions of Y-QL share this contribution.

REFERENCES

- Appenzeller I., Tscharnuter W., 1974, *A&A*, 30, 423
 Arnett W. D., 1977, *ApJ Suppl. Ser.*, 35, 145
 Bethe H. A., 1993, *ApJ*, 412, 192
 Bethe H. A., 1995, *ApJ*, 449, 714
 Bian F.-Y., Lou Y.-Q., 2005, *MNRAS*, 363, 1315
 Bionta R. M., et al., 1987, *Phys. Rev. Lett.*, 58, 1494
 Bodenheimer P., Sweigart A., 1968, *ApJ*, 152, 515
 Boily C. M., Lynden-Bell D., 1995, *MNRAS*, 276, 133
 Bond J. R., Arnett W. D., Carr B. J., 1984, *ApJ*, 280, 825
 Bouquet S., Feix M. R., Fualkow E., Munier A., 1985, *ApJ*, 293, 494
 Brown G. E., Bethe H. A., 1994, *ApJ*, 423, 659
 Burrows A., 2000, *Nature*, 403, 727
 Chandrasekhar S., 1957, *Stellar Structure*. Dover Publications, New York
 Cheng A. F., 1978, *ApJ*, 221, 320
 Fatuzzo M., Adams F. C., Myers P. C., 2004, *ApJ*, 615, 813
 Fillmore J. M., Goldreich P., 1984, *ApJ*, 284, 1
 Foster P. N., Chevalier R. A., 1993, *ApJ*, 416, 303
 Goldreich P., Weber S. V., *ApJ*, 1980, 238, 991
 Herrero A., Kudritzki R. P., Vilchez J. M., Kunze D., Butler K., Haser S., 1992, *A&A*, 261, 209
 Hirata K. S., et al., 1987, *Phys. Rev. Lett.*, 58, 1490
 Hu J., Shen Y., Lou Y.-Q., Zhang S.N., 2006, *MNRAS*, 365, 345
 Hunter C., 1977, *ApJ*, 218, 834
 Hunter C., 1986, *MNRAS*, 223, 391
 Jordan D. W., Smith P., 1977, *Nonlinear Ordinary Differential Equations*, Oxford University Press. Oxford
 Kennel C. F., Coroniti F. V., 1984, *ApJ*, 283, 694
 Landau L. D., Lifshitz E. M., 1959, *Fluid Mechanics*, Pergamon Press, New York
 Larson R. B., 1969a, *MNRAS*, 145, 271
 Larson R. B., 1969b, *MNRAS*, 145, 405
 Lattimer J. M., Prakash M., 2004, *Science*, 304, 536
 Lou Y.-Q., 2005, *ChJAA*, 5, 6
 Lou Y.-Q., Shen Y., 2004, *MNRAS*, 348, 717
 Lou Y.-Q., 2005, *ChJAA*, 5, 6
 Lou Y.-Q., Gao Y., 2006, *MNRAS*, submitted
 McLaughlin D. E., Pudritz R. E., 1997, *ApJ*, 476, 750
 Murakami M., Nishihara K., Hanawa T., 2004, *ApJ*, 607, 879

- Nadyozhin D. K., Razinkova T. L., 2005, *Astronomy Letters*, 31, 695 (astro-ph/0505056)
- Nauenberg M., Chapline G., 1973, *ApJ*, 179, 277
- Ori A., Piran T., 1988, *MNRAS*, 234, 821
- Penston M. V., 1969a, *MNRAS*, 144, 425
- Penston M. V., 1969b, *MNRAS*, 145, 457
- Press W. H., Flannery B. P., Teukolsky S. A., Vetterling W., 1986, *Numerical Recipes* (Cambridge: Cambridge University Press)
- Rhoades C. E., Ruffini R., 1974, *Phys. Rev. Lett.*, 32, 324
- Schaller G., Schaerer D., Meynet G., Maeder A., 1992, *A&A Suppl. Ser.*, 96, 269
- Schönberner D., Harmanec P., 1995, *A&A*, 294, 509
- Semelin B., Sanchez N., de Vega H. J., 2001, *Phys. Rev. D*, 63, 4005
- Shapiro S. L., Teukolsky S. A., 1983, *Black Holes, White Dwarfs and Neutron Stars*, John Wiley & Sons, Inc.
- Shen Y., Lou Y. Q., 2004, *ApJL*, 611, L117
- Shen Y., Lou Y. Q., 2006, *MNRAS Lett*, 370, L85 (astro-ph/0605505)
- Shu F. H., 1977, *ApJ*, 214, 488
- Shu F. H., Lizano S., Galli D., Cantó J., Laughlin G., 2002, *ApJ*, 580, 969
- Suto Y., Silk J., 1988, *ApJ*, 326, 527
- Terebey S., Shu F. H., Cassen P., 1984, *ApJ*, 286, 529
- Tsai J. C., Hsu J. J. L., 1995, *ApJ*, 448, 774
- Wang W. G., Lou Y.-Q., 2006, *MNRAS*, submitted
- Whitworth A., Summers D., 1985, *MNRAS*, 214, 1
- Yahil A., 1983, *ApJ*, 265, 1047
- Yu C., Lou Y.-Q., 2005, *MNRAS*, 364, 1168
- Yu C., Lou Y.-Q., Bian F. Y., Wu Y., 2006, *MNRAS*, 370, 121 (astro-ph/0604261)

APPENDIX A: POLYTROPIC CASES OF $\gamma \geq 4/3$

When index $\gamma > 4/3$ is adopted for a polytropic gas, the self-similar transformation should be modified slightly. In fact, the only difference between this case and what we have considered in the main text concerns the transformation for the total enclosed mass M . As $M > 0$ is a physical requirement in transformation (7), the scaling factor e should take the form of

$$e = \frac{k^{3/2} t^{3n-2}}{(2-3n)G} \quad (\text{A1})$$

for $\gamma > 4/3$ in a parallel analysis. For example, the $nx-v > 0$ criterion for $m > 0$ should now be replaced by $nx-v < 0$.

The $\gamma = 4/3$ case is special and makes the scaling factor e in definition (7) meaningless. Noting that the factor $3n-2$ was only added for convenience, we may simply set

$$e = \frac{k^{3/2}}{G} \quad (\text{A2})$$

to perform a self-similar transformation. Substituting this modified transformation into hydrodynamic equations (1) through (5) under spherical symmetry, we obtain

$$v = nx = 2x/3, \quad (\text{A3})$$

$$m' = \alpha x^2, \quad (\text{A4})$$

and a second-order nonlinear ODE for α alone

$$\alpha'' + \frac{2\alpha'}{x} - \frac{2(\alpha')^2}{3\alpha} - \frac{1}{2}\alpha^{2/3} + \frac{3}{4}\alpha^{5/3} = 0. \quad (\text{A5})$$

We shall pursue a more complete analysis of this problem in a separate paper.